



UNIVERSITY OF GENOA

MASTER'S PROGRAM IN BIOENGINEERING

Thesis submitted in partial fulfillment of the requirements for the title of
Master of Bioengineering

A multiscale computational model of Deep Brain Stimulation of the Anterior Nucleus of the Thalamus for epilepsy treatment

Lorenzo Prione

March 2025

Thesis advisor: Dr. rer. nat Maria Carla Piastra

Thesis advisor: Prof. Sergio Martinoia

Thesis co-advisor: Msc. Nadezhda Chaplinskaia

List of Abbreviations

General Neurophysiology & Epilepsy

- **AED** = Anti Epileptic Drug
- **CT** = Computed Tomography
- **DRE** = Drug-Resistant Epilepsy
- **EEG** = Electroencephalography
- **EP** = Evoked Potential
- **EPSP** = Excitatory Post-Synaptic Potential
- **fMRI** = Functional Magnetic Resonance Imaging
- **IPSP** = Inhibitory Post-Synaptic Potential
- **MEG** = Magnetoencephalography
- **MRI** = Magnetic Resonance Imaging
- **PNES** = Psychogenic Non-Epileptic Seizure
- **PSP** = Post-Synaptic Potential

Deep Brain Stimulation & Neuromodulation

- **ANT** = Anterior Nucleus of the Thalamus
- **AP** = Action Potential
- **DBS** = Deep Brain Stimulation
- **GABA** = Gamma-Aminobutyric Acid
- **GPi** = Globus Pallidus Internus
- **NMDA** = N-Methyl-D-Aspartate
- **STN** = Subthalamic Nucleus
- **VNS** = Vagus Nerve Stimulation

Computational Modeling & Inference

- **BNM** = Brain Network Model
- **NMM** = Neural Mass Model
- **SA** = Sensitivity Analysis
- **SBI** = Simulation Based Inference
- **SNPE** = Sequential Neural Posterior Estimation
- **TVB** = The Virtual Brain

Epilepsy is a chronic neurological disorder that causes recurrent seizures, with about 30% of patients suffering from drug-resistant epilepsy. Not all patients are suitable for surgery, and some continue to experience seizures even afterwards. In these cases, neuromodulation techniques like Deep Brain Stimulation should be considered. Research has demonstrated the efficacy of bilateral Deep Brain Stimulation of the Anterior Nucleus of the Thalamus in reducing seizures, though its underlying mechanisms are not fully understood. Computational modeling offers a way to explore these mechanisms and optimize stimulation settings.

We implemented a multiscale computational model using The Virtual Brain to simulate the effects of Deep Brain Stimulation of the Anterior Nucleus of the Thalamus for epilepsy treatment. A sanity check was conducted to validate the model's suitability for this application, and the simulated data were compared with electroencephalographic recordings from the EANSkE project to assess biological plausibility. A sensitivity analysis of the Jansen-Rit parameters was performed to identify those most influential on the model's output.

The model reproduced the expected dynamics of the Jansen-Rit single cortical column model within the complex environment of The Virtual Brain, confirming its suitability for our purposes. Analysis of simulated data using Global Mean Field Power and topographical plots, supported by qualitative comparison with real data, confirmed biological plausibility. Sensitivity analysis in two simulation settings identified key parameters influencing the results.

These findings confirm the feasibility of using the Jansen-Rit model within The Virtual Brain to study Deep Brain Stimulation effects. The model produced biologically plausible signals, supported by real data. The sensitivity analysis highlighted parameters crucial for future investigations. The proposed pipeline is ready for integration with customized connectivity.

Contents

1	Introduction	15
1.1	Neurophysiology of epilepsy	15
1.1.1	Classification of seizures	16
1.1.2	Pathophysiology	16
1.1.3	Diagnosis	18
1.1.4	Treatment	19
1.2	Deep Brain Stimulation	20
1.2.1	Neurophysiology of Deep Brain Stimulation	21
1.2.2	Anterior Nucleus of the Thalamus	22
1.2.3	Stimulation parameters	23
1.3	Evoked Potentials	25
1.4	Computational modeling	26
1.4.1	Computational models of epilepsy	26
1.4.2	Neural Mass Models	28
1.4.3	Jansen-Rit Model	29
1.4.4	Transition of J-R to a more generalized model	33
1.4.5	The Virtual Brain	34
1.5	Simulation-Based Inference	36
1.5.1	Sequential Neural Posterior Estimation	37

1.5.2	Sensitivity Analysis with SBI	38
1.6	Research goal	43
2	Materials and method	45
2.1	Clinical Data	45
2.2	Setup of TVB with DBS	48
2.2.1	Nodes	48
2.2.2	Connectivity	50
2.2.3	Projection matrix	51
2.3	Jansen-Rit sanity check	52
2.4	TVB simulation	55
2.4.1	Artifact	55
2.4.2	Evoked Potentials	60
2.5	Qualitative comparison with clinical EEG	61
2.6	Sensitivity analysis	65
3	Results	67
3.1	Jansen-Rit sanity check	67
3.2	Simulated data	71
3.3	Qualitative comparison with real data	75
3.4	Sensitivity Analysis	80
4	Discussion	87
4.1	Key findings	87
4.2	Comparison with existing studies	92
4.3	Limitations and Future Work	96
5	Conclusion	99

6 Acknowledgements	101
Bibliography	102

“I would rather have questions that can’t be answered
than answers that can’t be questioned.”

– Richard P. Feynman

Introduction

1.1 Neurophysiology of epilepsy

Epilepsy, also known as seizure disorder [Mayo Clinic, 2023], is a common chronic neurological disorder characterized by recurrent and unprovoked epileptic seizures, resulting from abnormal and excessive synchronized electrical signals produced by damaged brain cells [Kirchner *et al.*, 2020], [Cleveland Clinic, 2022].

Epilepsy is common, approximately 50 million people worldwide suffer from it, and about 30 to 40% of these have seizures that are refractory to treatment with antiepileptic medication [González *et al.*, 2019].

The term "epileptic seizure" is used to distinguish seizures caused by short-lived, and therefore inherently non-chronic secondary reversible conditions such as fever or Psychogenic Non-epileptic Seizure (PNES) [National Institute of Neurological Disorders and Stroke, 2025].

The disease, particularly in its chronic stage, significantly influences the quality of life of the sufferers [Strzelczyk *et al.*, 2023].

1.1.1 Classification of seizures

Seizures are classified as generalized, focal, and epileptic spasms. The classification is based on the onset region or origin of the seizure. A person with epilepsy can have more than one type of seizure [Stafstrom and Carmant, 2015].

Focal seizures originate in neuronal networks limited to one cerebral hemisphere. Their clinical manifestations depend on the area of the cortex involved and can cause changes in awareness, behaviour, or sensation on one side of the body. This type of seizure can spread to both hemispheres and, when this happens, it can cause loss of consciousness. These just described are, respectively, focal-onset aware seizures and impaired awareness seizures [Scheffer *et al.*, 2017].

Generalized seizures begin in bilaterally distributed neuronal networks at the same time. Usually, they are characterized by a loss of consciousness or awareness and can also cause abnormal movements on both sides of the body. They are called generalized non-motor (absence) and motor (tonic-clonic) seizures. The first was known as "petit mal" and are relatively short, sudden lapse of consciousness; the second was known as "grand mal" and causes a person to lose awareness and have muscle movements of different entities and combinations [Fisher, 2017] [Stafstrom and Carmant, 2015].

Epileptic spasms have unknown onset and do not fit in any of the two categorizations due to incomplete information. They are sudden extensions or flexions of the extremities that recur in clusters [Goldstein and Slomski, 2008].

1.1.2 Pathophysiology

A seizure can be conceptualized as occurring when there is a distortion of the normal balance between excitation (E) and inhibition (I) in the brain [Stafstrom and Carmant, 2015]. This distortion can be genetic or acquired; while the first type

can occur anywhere from the circuit level to the receptor level, the second mainly concerns a cerebral insult that can alter the circuit function. The developing brain is particularly prone to seizures since excitatory synaptic function develops before inhibitory synaptic function [Rho *et al.*, 2010].

Hypersynchronous discharges during a seizure can begin in a very discrete cortex region and then spread to neighbouring regions. Seizure initiation is characterized by two concurrent events: high-frequency bursts of action potentials (APs), and hypersynchronization of a neuronal population [Bromfield *et al.*, 2006]. The synchronized bursts from a sufficient number of neurons result in a so-called spike discharge on the electroencephalogram (EEG).

The EEG is the registration of neuronal activity within the human brain and reflects changes in the cell's resting membrane potential, which is measured negatively against the extracellular space. Whereas APs are too short to adequately sum up, postsynaptic potentials (PSPs) with durations of up to several 10 ms are capable of producing potential changes to be recorded extracellularly on the scalp [Kirschstein and Köhling, 2009].

At the cellular level, epileptiform activity includes a paroxysmal depolarizing shift, characterized by a plateau-like depolarization that triggers APs, followed by repolarization and hyperpolarization [Rho *et al.*, 2010]. This activity is due to the influx of Ca^{2+} and Na^+ ions and is regulated by GABA receptors and ion channels. Seizures then spread by recruiting surrounding neurons through increased extracellular K^+ , increased neurotransmitter release, and activation of NMDA receptors.

Two main theories aim to explain the hyperexcitability of the hippocampus, a common site for partial seizures: loss of inhibitory interneurons and synaptic reorganization. Moreover, generalized seizures can arise from abnormal oscillatory rhythms in the cortex-thalamus circuits [Bromfield *et al.*, 2006].

1.1.3 Diagnosis

The history and neurologic examination are the cornerstones of the diagnosis of seizures and epilepsy, which will evaluate focal signs that could implicate or localize cerebral pathology [Stafstrom and Carmant, 2015].

An EEG measures the brain's electrical activity and is used to detect abnormal patterns, such as focal spikes or waves indicative of epilepsy. Routine EEGs should include periods of wakefulness, drowsiness, and sleep, as epileptiform activity varies with these states. In some cases, intracranial EEG (iEEG) monitoring is necessary, particularly when the seizure focus is in hard-to-detect areas like the frontal or temporal lobes. While EEG findings support the diagnosis, they are not definitive; clinical information remains paramount [Benbadis, 2009] [Stafstrom and Carmant, 2015].

Computed Tomography (CT) and Magnetic Resonance Imaging (MRI) scans are fundamental in evaluating possible structural brain lesions that may underlie seizures. Usually, MRI is preferred for its higher sensitivity, especially in detecting subtle abnormalities like cortical malformations or hippocampal sclerosis. Advanced imaging techniques, such as functional MRI (fMRI) and magnetoencephalography (MEG), provide further insights into brain function and seizure localization [Pelinen *et al.*, 2024] [Stafstrom and Carmant, 2015].

The extent of metabolic testing depends on the type of seizure and epilepsy syndrome.

As the genetic foundations of epilepsy become clearer, genetic testing is becoming increasingly important in clinical settings. Available tests range from basic karyotyping to identify chromosomal anomalies, to targeted gene panels for specific syndromes, like sodium channel protein type 1 subunit alpha (SCN1A) for Dravet syndrome [Krey *et al.*, 2022].

1.1.4 Treatment

About 30–40% of the worldwide epileptic patients have seizures that are refractory to treatment with anti-epileptic drugs (AEDs), which usually is the first-line treatment [González *et al.*, 2019].

The diagnosis of drug-resistant epilepsy (DRE) should be confirmed and acted on promptly to control seizures: surgery is a highly effective treatment for DRE, where 65% of patients with focal epilepsy achieve sustained seizure remission after surgical therapy [Wiebe and Jette, 2012]. However, not all persons are candidates for epilepsy surgery. Furthermore, despite careful selection, some of them may continue to experience seizures postoperatively.

In this case and in all other cases where secondary routes of treatment fail, neuromodulation-based interventions, such as Vagus Nerve Stimulation (VNS) or Deep Brain Stimulation (DBS) which have proven to be extremely effective in the treatment of DRE, should be considered [Litvak *et al.*, 2021].

1.2 Deep Brain Stimulation

Deep Brain Stimulation is an adjustable, effective neuromodulatory treatment method for patients with DRE, involving the implantation of stimulating electrodes in subcortical structures and, in a later stage, chronic stimulation of these structures with an implantable pulse generator. The latter, during brain stimulation, directly generates and delivers an electrical current to the brain tissue through the intracranial electrodes [Litvak *et al.*, 2021].

In VNS, instead, surgeons insert a wire threaded under the skin that connects the stimulating device to the left vagus nerve. The device sends electrical signals along the left vagus nerve to the brainstem affecting the brain. The vagus nerve on the right side of the body is not often used because it's more likely to affect how the heart works [Mayo Clinic, 2024].

In DBS, these electrodes are surgically implanted either cortically on the surface target or penetrating deep into the brain tissue, using strip or depth electrodes respectively.

The electrical current flow is produced either as a monopolar between one electrode and reference, bipolar between electrodes, or multipolar between several electrode contacts. Several parameters define the shape of the stimulus, including current amplitude, pulse width, burst duration, and frequency. Open-loop stimulation devices, such as DBS, deliver continuous periodic stimulation to the brain.

The stimulation settings are adjusted empirically in a trial-and-error fashion until an acceptable response is achieved [Foutz and Wong, 2022].

1.2.1 Neurophysiology of Deep Brain Stimulation

The DBS electric field is a complex three-dimensional phenomenon distributed throughout the brain. It is generated by the redistribution of charged ions in the extracellular space as a result of electrode polarization.

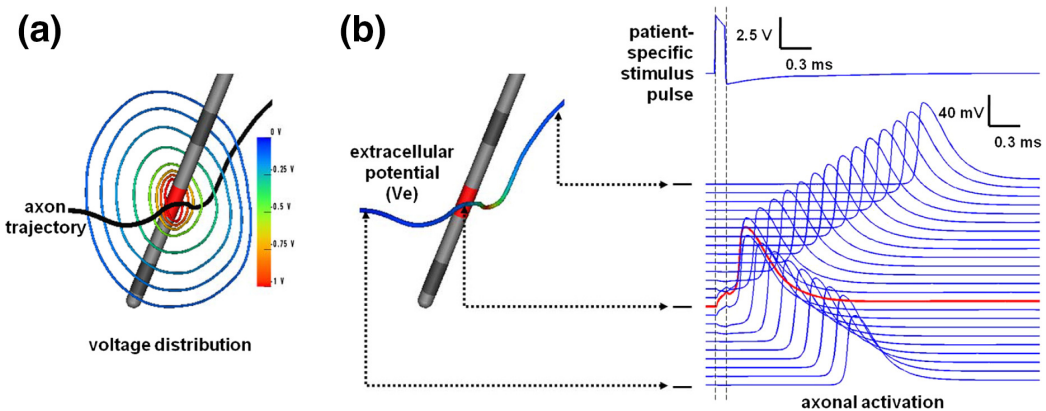


Figure 1.1: Neural response to stimulation, DBS electrodes generate a nonlinear voltage gradient, polarizing nearby axons based on their position and stimulus strength; sufficient stimulation triggers bidirectional APs [McIntyre and Anderson, 2016]

The fundamental purpose of the applied electric field on the neuronal process is to induce a transmembrane voltage change that can open voltage-gated sodium channels on the axon. The cathodic phase of the stimulus pulse generates a membrane depolarization at the Ranvier nodes closest to the electrode contact [McIntyre and Anderson, 2016].

Once APs are generated, they typically propagate to their axon terminals and induce neurotransmitter release. In turn, each AP, in each directly stimulated neuron, can result in hundreds of synaptic events throughout the complex axonal arbor of that neuron. All of those DBS-induced synaptic events can alter the balance of neurotransmitters within the stimulated brain network.

The effects of electric fields on axons are non-discriminatory to the type of neurotransmitter used by any particular pathway. So, depending on the specific pathway being stimulated, the effect could be either inhibitory via modulated GABA release or excitatory via modulated glutamate release [McIntyre and Anderson, 2016].

1.2.2 Anterior Nucleus of the Thalamus

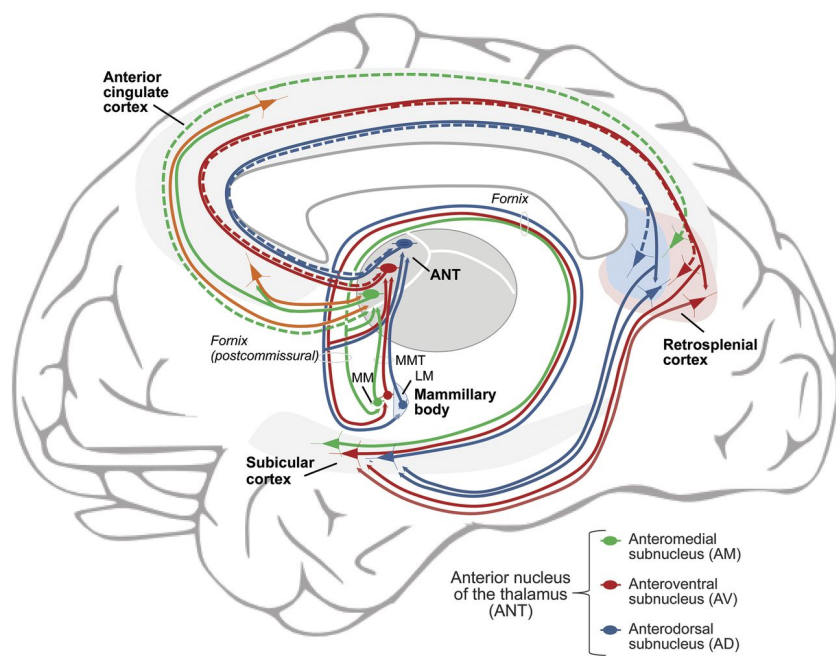


Figure 1.2: Main connections of the anterior nucleus of the thalamus (ANT) and subnuclei with distinct connectivity [Child and Benarroch, 2013]

The anterior nucleus of the thalamus (ANT) is a key component of the hippocampal system for episodic memory. The ANT consists of 3 subnuclei with distinct connectivity with the subiculum cortex, retrosplenial cortex, and mammillary bodies. Via its connections with the anterior cingulate and orbitomedial pre-

frontal cortex, the ANT can also contribute to reciprocal hippocampal-prefrontal interactions involved in emotional and executive functions [Child and Benarroch, 2013].

As in other thalamic nuclei, ANT neurons have two different state-dependent patterns of discharge, tonic and burst-firing; some ANT neurons also contribute to the propagation of the theta rhythm, which is important for the synaptic plasticity mechanisms of the hippocampal circuit [Child and Benarroch, 2013].

Because of its central connectivity and possible role in the propagation of seizure activity, the ANT has become an attractive target for DBS for the treatment of medically refractory epilepsy [Laxpati *et al.*, 2014].

Pioneering studies on rhesus monkeys indicated that ANT plays a role in the generalization of focal cortical seizures, this is supported by pharmacological studies showing that increased activation of GABA receptors in ANT suppressed high voltage synchronous EEG activity and behavioural components of generalized seizures [Mahrous *et al.*, 2025].

1.2.3 Stimulation parameters

As there is no universally known set of stimulation parameters, they are currently chosen empirically, taking into account the experience of various researchers and their studies, such as the Stimulation of the Anterior Nucleus of the Thalamus for Epilepsy (SANTE) [Fisher *et al.*, 2010]. The study investigates the efficacy and possible side effects of ANT stimulation in patients with drug-resistant epilepsy.

The effects of varying the main parameters of stimulation, such as frequency, voltage and current intensity, pulse width, unilateral versus bilateral stimulation, and cyclic versus continuous stimulation, are currently a question mark in this field of neuroscience. Generally speaking, low-frequency stimulation is believed

to increase the risk of seizures by lowering the seizure threshold and enhancing epileptogenic discharges, while higher frequencies (≥ 100 Hz) desynchronise electrical activity and reduce the risk of seizures.

The only thing that seemed to change the results from the SANTE study was the exact positioning of DBS electrodes appearing significant as ANT-DBS electrodes located anteriorly, or in the antero-ventral subdivision of the ANT were correlated with a better outcome.

At 7 years from the SANTE study [Salanova *et al.*, 2021], median seizure frequency percent reduction from baseline was 75% ($p < .001$), with no outcome differences related to prior vagus nerve stimulation or resective surgery. The most severe seizure type, focal to bilateral tonic-clonic, was reduced by 71%.

1.3 Evoked Potentials

An evoked potential (EP) is the averaged electrical activity recorded from the scalp (e.g., with EEG), often only several microvolts in amplitude, that is elicited in response to a stimulus [Challenor *et al.*, 1994]. One example of such is the current injected by DBS, which can evoke characteristic electrophysiological responses in neural circuits.

The potential that is evoked is time-locked to the stimulus in contrast to random spontaneous electrical fluctuations such as electroencephalographic activity or other electrical noise [Fifer *et al.*, 2006]. The scalp electrode receives the electrical volley generated by an electrical stimulus from relatively far away and records multiple peaks as the volley traverses various anatomic structures in this far-field recording, in contrast to the immediacy of the triphasic, near-field response obtained with electrodes sitting directly over a nerve conducting a nerve AP.

The available scientific literature regarding the presence of evoked potentials following ANT-DBS is far from abundant. Nevertheless, there are some groups such as [Wang *et al.*, 2020] that applied 2 Hz DBS in the ANT resulting in strong EPs as well as weak EPs in some of the participants or [Yu *et al.*, 2018] in which, with a 1 Hz stimulation, the effective connectivity between the hippocampus and ANT was evaluated using hippocampal-thalamic EPs and thalamic-hippocampal EPs in six patients with mesial temporal seizure onset.

More literature on the matter exists regarding stimulation of the subthalamic nucleus (STN) or Globus Pallidus internus (GPi) in Parkinsonians where DBS has been reported to be successful in relieving the core motor symptoms of Parkinson's disease (PD) and motor fluctuations in the more advanced stages of the disease [Skodda, 2012] [Odekerken *et al.*, 2015].

1.4 Computational modeling

New experimental technologies give us the ability to observe neurons, networks, brain regions, and whole systems at unprecedented scale and resolution, but using these data to understand how behaviour arises from neural processes remains a challenge. To test our understanding of a phenomenon, we often take to rebuilding it in the form of a computational model that incorporates the mechanisms we believe to be at play, based on scientific knowledge, intuition, and hypotheses about the components of a system and the laws governing their relationships.

The goal of such models is to investigate whether a proposed mechanism can explain experimental data, uncover details that may have been missed, inspire new experiments, and eventually provide insights into the inner workings of an observed neural or behavioural phenomenon [Gonçalves and Lueckmann, 2020].

1.4.1 Computational models of epilepsy

Computational models of epilepsy aim to approximate and understand the mechanisms underlying epileptic activity by mathematically representing different components of the brain through differential equations.

Computational models relevant to epilepsy exist in many forms, from macroscopic mean-field models of seizure dynamics to detailed neural network models of network activity to intricate ion channel models of epileptogenic ion channel mutations [Case and Soltesz, 2011].

Their ability to operate across multiple scales, from microscopic (single neuronal dynamics) to macroscopic (whole brain activity), is a key advantage that allows researchers to bridge gaps between cellular abnormalities and large-scale network dysfunction.

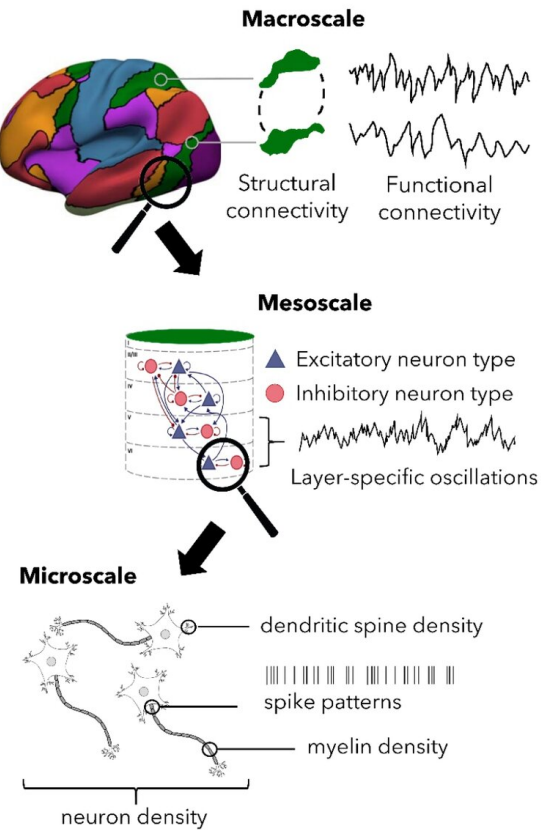


Figure 1.3: Different scales of brain organization in multiscale connectomic modeling: macroscale, mesoscale and microscale [Haueis, 2022]

Computational modeling also has direct clinical applications: models have been used in implantable devices designed to detect seizures and deliver targeted electrical stimulation to suppress them [Jobst *et al.*, 2010]. By integrating patient-specific data, these models have the potential to personalize epilepsy research and treatment strategies, paving the way for more personalized therapeutic interventions.

1.4.2 Neural Mass Models

The brain is characterized by a complex behaviour that spans different time-space scales. Due to this peculiarity, a mesoscopic approximation can simulate large-scale brain network models and their macroscopic spatiotemporal dynamics.

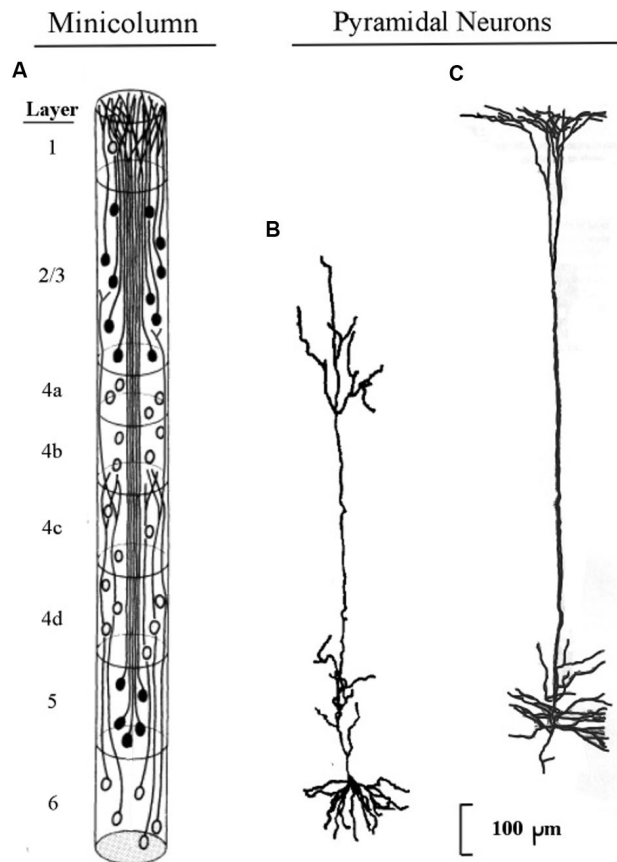


Figure 1.4: Graphical representation of minicolumn and pyramidal neurons [LaBerge and Kasevich, 2017]

This approximation makes use of pools of cortical neurons that share similar characteristics aggregate to form regions known as cortical columns or macro-

columns [Jirsa and Stefanescu, 2011], [Schwalger *et al.*, 2017].

The temporal behaviour of these structures is described by a system of differential equations, which serves as a mathematical translation of the ensembles of neurons. The structures above are characterized by models developed using a mass action approach, where clusters of neurons that share similar characteristics form neural masses.

A Brain Network Model (BNM) (also referred to as a graph-based brain anatomical network) describes the mesoscopic and macroscopic dynamics of cortical neural activity, potentially including thalamic and other non-cortical structures [Sanz-Leon *et al.*, 2015]. Given the dimensionality of these models, they are often analytically intractable, and therefore numerical simulations are essential for providing insights about their behaviour.

The generic BNM also encompasses an alternative and discrete approach to neural-field modeling by using dense networks of neural masses on a mesh.

1.4.3 Jansen-Rit Model

Jansen-Rit is a neurophysiological mass model used to describe cortical column dynamics in the brain, with its focus on how neural populations generate oscillatory activity and process signals [Jansen and Rit, 1995].

To describe cortical activity, a nonlinear model should be used, since it has been proven mechanisms beyond the oscillation generation in the brain to be nonlinear. A neural mass model (NMM) provides the possibility of reducing the complexity of the dynamics within cortical connections to one of relatively simple circuits. Jansen-Rit has subsequently undergone further development to understand different types of brain activities, among which visual evoked potentials (VEPs).

The operability of the model is contingent upon the representation of a popu-

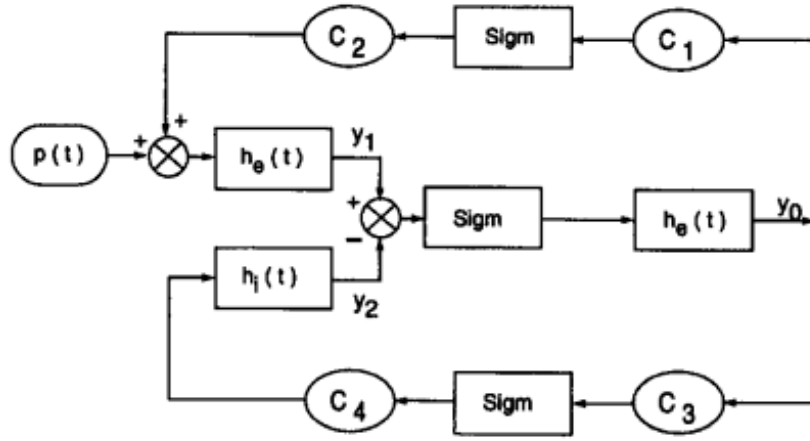


Figure 1.5: Simplified model of Jansen-Rit single cortical column model for cortical alpha wave generation [Jansen and Rit, 1995]

lation of "feedforward" pyramidal cells that receive either excitatory or inhibitory inputs from local interneurons (i.e., other pyramidal, stellate, or basket cells within the same column) as well as excitatory input from neighbouring or farther columns. The latter input is represented by a pulse density $p(t)$, which can be any arbitrary function.

Each neuronal population is modelled by two blocks, the first transforms $p(t)$ into an average post-synaptic membrane potential (which can be either inhibitory or excitatory). It is called PSP block and represents a linear transformation with an impulse response given by

$$h_e(t) = \begin{cases} A a t e^{-at} & t \geq 0 \\ 0 & t < 0 \end{cases} \quad (1.1)$$

for the excitatory case, and

$$h_i(t) = \begin{cases} B b t e^{-at} & t \geq 0 \\ 0 & t < 0 \end{cases} \quad (1.2)$$

for the inhibitory case. A and B represent the parameters determining respectively the maximum excitatory and inhibitory post-synaptic potential (EPSP and IPSP).

Whilst, a and b are the lumped representations of the sum of the reciprocal of the time constant of the passive membrane and all other spatially distributed delays in the dendritic network.

The second block incorporates a sigmoid function to transform the average membrane potential of neurons into an average pulse density of APs. The function is expressed as:

$$Sigm(v) = \frac{2e_0}{1 + e^{r(v_0 - v)}} \quad (1.3)$$

where e_0 indicates the maximum firing rate, v_0 is the membrane potential for a 50% firing rate, and r represents the steepness of the curve.

The interaction between pyramidal cells and interneurons is characterized by the four connectivity constants C_1 through C_4 , which account for the total number of synapses established by interneurons onto the axons and dendrites of the neurons constituting the cortical column.

The model employs a set of six differential equations to describe the interactions between inputs ($x(t)$) and outputs ($y(t)$) of the neurons:

$$\dot{y}_0(t) = y_3(t) \quad (1.4)$$

$$\dot{y}_3(t) = Aa \operatorname{Sigm}[y_1(t) - y_2(t)] - 2ay_3(t) - a^2y_0(t) \quad (1.5)$$

$$\dot{y}_1(t) = y_4(t) \quad (1.6)$$

$$\dot{y}_4(t) = Aa\{p(t) + C_2 \operatorname{Sigm}[C_1 y_0(t)]\} - 2ay_4(t) - a^2y_1(t) \quad (1.7)$$

$$\dot{y}_2(t) = y_5(t) \quad (1.8)$$

$$\dot{y}_5(t) = Bb\{C_4 \operatorname{Sigm}[C_3 y_0(t)]\} - 2by_5(t) - b^2y_2(t) \quad (1.9)$$

where y_0 (1.4), y_1 (1.6), and y_2 (1.8) are the outputs of the three PSP blocks, respectively.

Parameter	Value
A	3.25
B	22
C	135
v_0	6

Table 1.1: Set of standard values for the model parameters of the cortical column for cortical alpha wave generation

In a single cortical column, the model demonstrated the possibility, by varying the connectivity constants, to produce different types of neural oscillation, from noise to alpha rhythms (8-13 Hz) and to transition through various states, which are dependent on the other parameters. The alpha-like activity observed for $C = 135$ led to the definition of a set of standard values for the model parameters of the visual cortical column, which are visible in Table 1.1.

In a dual-column model where the two cortical columns are coupled even with

minimal connectivity, the oscillatory activity tends to synchronise, while for different cortical areas, by varying parameters and introducing temporal phase delays, alpha and beta rhythms can be replicated.

Again, using the dual-column model, in the case of studying EPs, it is shown how the interaction between columns influences the complexity of the response to a stimulus.

The model applies correctly to the study we want to perform, being applicable for a brain stimulation protocol concerning the prediction of how different cortical areas may respond to stimulation depending on their connectivity.

1.4.4 Transition of J-R to a more generalized model

Although [Jansen and Rit, 1995] doesn't directly address how the model can be generalized to reproduce an EEG signal that includes all oscillatory modes (delta, theta, gamma, etc.), it surely alludes to the mechanisms to do it and implies that it is feasible via a parameter tuning (connectivity constants, synaptic time constants, external input properties).

Since it captures the fundamental mechanisms underlying cortical rhythms, the NMM's design inherently supports the exploration of a wide range of oscillatory dynamics.

So, by modulating the values of synaptic time constants, the gains (whether excitatory or inhibitory depending on the case) of the connectivity strengths that influence the amplitude and frequency of oscillations, and the frequency content and strength of the external input, specific oscillatory patterns that go beyond alpha and beta oscillations can be induced.

1.4.5 The Virtual Brain

The Virtual Brain (TVB) thevirtualbrain.org is an open-source cutting-edge neuroinformatics platform that finds its fundamental purpose in providing a framework for simulating and analyzing neural networks ranging from single neurons to entire brain-scale models which describe the brain as a graph composed of nodes that represent brain areas and edges that represent physical connections between these areas, making this accessible and understandable to researchers with different backgrounds.



THE VIRTUAL BRAIN.

Figure 1.6: The Virtual Brain logo thevirtualbrain.org

Users can conduct multi-scale simulations, beginning with specific mathematical models and subsequently generating sufficiently accurate simulations of EEG, MEG, blood oxygenation level-dependent (BOLD), and stereo EEG (sEEG) signals through methods from statistical physics. The key to producing these results is a hybrid approach that merges individual anatomy from brain imaging data with mathematical modeling.

One of the significant advantages of TVB as a simulation software is its re-

markable ease of use and the flexibility of its kernel, which allows researchers to efficiently manipulate the model by adjusting external parameters or the nodes and connectivity of the network, enabling rapid modifications through an intuitive interface.

1.5 Simulation-Based Inference

A crucial step in getting a model to agree with experimental data is adjusting its free parameters. This is essential for learning more about processes that are impossible to quantify through experimentation as well as for determining whether the model accurately represents reality. For some models in neuroscience, this is possible from careful mathematical analysis of the model equations. But as the complexity of both neural data and neural models increases, it becomes very difficult to find well-fitting parameters by inspection, and automated identification of data-consistent parameters is required [Gonçalves and Lueckmann, 2020].

Moreover, to grasp how a model quantitatively explains data, it is necessary to find not only the best but all parameter settings consistent with experimental observations. This is true especially when modeling neural data, where highly variable observations can lead to broad ranges of data-consistent parameters. Furthermore, many models in biology are inherently robust to some perturbations of parameters, but highly sensitive to others (for example because of processes such as homeostatic regulation).

The starting point for automated parameter identification is statistical inference:

$$p(\theta|x) = \frac{p(x|\theta)p(\theta)}{p(x)} \quad (1.10)$$

which uses the likelihood $p(x|\theta)$ to quantify the match between parameters θ and data x . Likelihoods can be efficiently computed for purely statistical models commonly used in neuroscience, but are computationally intractable for most mechanistic models.

These latter are intended to reflect knowledge about biological mechanisms, and not necessarily to be amenable to efficient inference: many mechanistic mod-

els are defined implicitly through stochastic computer simulations and likelihood calculation would require the ability to integrate over all potential paths through the simulator code.

Similarly, a common goal of mechanistic modeling is to capture selected summary features of the data not the full dataset in all its details. The same feature can be produced by infinitely many realizations of the simulated process. This makes it impractical to compute likelihoods, as one would have to average over all possible realizations which produce the same output.

Thus, computational neuroscientists face a dilemma: either create carefully designed, highly interpretable mechanistic models (but rely on ad-hoc parameter tuning), or resort to purely statistical models offering sophisticated parameter inference but limited mechanistic insight.

To meet this challenge, there is an emerging set of techniques for simulation-based inference (SBI).

1.5.1 Sequential Neural Posterior Estimation

Sequential Neural Posterior Estimation (SNPE) is a tool that makes it possible to perform Bayesian inference on mechanistic models in neuroscience without requiring access to likelihoods. It identifies all mechanistic model parameters consistent with observed experimental data.

Given observed experimental data (or summary features) x_o and a mechanistic model with parameters θ it expresses both prior knowledge and the range of data-compatible parameters through probability distributions. SNPE returns a posterior distribution $p(\theta|x_o)$ which is high for parameters θ consistent with both the data x_o and prior knowledge, but approaches zero for θ inconsistent with either.

SNPE uses simulations instead of likelihood calculations, but instead of filter-

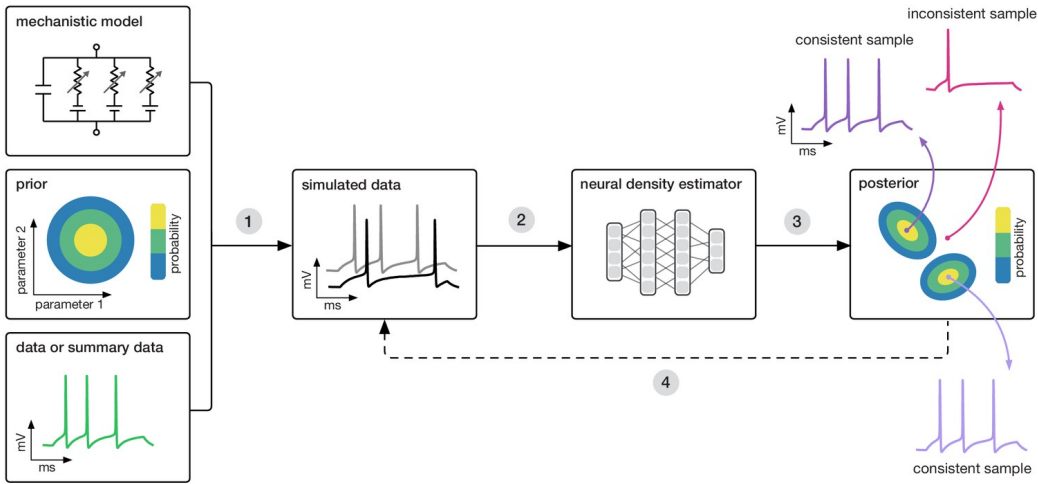


Figure 1.7: Diagram of functioning of Sequential Neural Posterior Estimator (SNPE) that uses simulations to train a multilayer artificial neural network to identify admissible parameters <https://sbi-dev.github.io/sbi/0.22/>

ing them out, it uses all to train a multilayer artificial neural network to identify admissible parameters. By incorporating modern deep neural networks for conditional density estimation, it can capture the full distribution of parameters consistent with the data, even when this distribution has multiple peaks or lies on curved manifolds.

1.5.2 Sensitivity Analysis with SBI

Sensitivity Analysis (SA) is defined as “a method to determine the robustness of an assessment by examining the extent to which results are affected by changes in methods, models, values of unmeasured variables, or assumptions” with the aim of identifying “results that are most dependent on questionable or unsupported assumptions” [Schneeweiss *et al.*, 2006].

It has also been defined as “a series of analyses of a data set to assess whether

altering any of the assumptions made leads to different final interpretations or conclusions” [Viel *et al.*, 1995] [Thabane *et al.*, 2013].

To achieve these objectives, the Active Subspace method [Constantine *et al.*, 2014] implemented in the SBI platform https://sbi-dev.github.io/sbi/0.22/tutorial/09_sensitivity_analysis/, to analyze the sensitivity of the parameters of the Jansen-Rit model, can be used. This approach relies on posterior distributions computed using the SBI SNPE.

The Active Subspace method identifies directions of strongest variability in the parameter space by evaluating the gradients of the function. These dominant directions are then used to construct a lower-dimensional response surface, reducing computational complexity while preserving key variability patterns.

We have our function $f(x)$ with m input parameters $x = (x_1, x_2, \dots, x_m)$ that in our case are respectively the posterior distribution of the parameters given a certain observed data and the parameters.

The gradient of f is denoted by the column vector:

$$\nabla_x f(x) = \begin{bmatrix} \frac{\partial f}{\partial x_1} \\ \frac{\partial f}{\partial x_2} \\ \vdots \\ \frac{\partial f}{\partial x_m} \end{bmatrix}$$

We evaluate this gradient at M sampled input points x_j , where $j = 1, \dots, M$.

The covariance matrix C of gradients $\nabla_x f$ is defined as:

$$C = \mathbb{E} [(\nabla_x f)(\nabla_x f)^T]$$

where \mathbb{E} is the expectation operator and it is assumed that f is such that C exists; or in other words, the products’ partial derivatives are integrable.

This expectation \mathbb{E} is estimated via Monte Carlo approximation with M samples:

$$C \approx \frac{1}{M} \sum_{j=1}^M \nabla_x f(x_j) \nabla_x f(x_j)^T$$

where M is the number of gradient evaluations and C is an $m \times m$ symmetric matrix, that can be interpreted as the uncentered covariance of the gradient vector.

Since C is symmetric and positive semidefinite, it admits a real eigenvalue decomposition:

$$C = W\Lambda W^T$$

where W is an $m \times m$ orthogonal matrix whose columns are the eigenvectors w_1, \dots, w_m and Λ is a diagonal matrix with the eigenvalues $\lambda_1, \lambda_2, \dots, \lambda_m$.

The eigenvalues λ tell us how much variance in $f(x)$ is associated with each eigenvector w . Large eigenvalues correspond to important directions that form the active subspace.

The eigenvectors are partitioned based on the dominant eigenvalues:

$$W = \begin{bmatrix} W_1 & W_2 \end{bmatrix}, \quad \Lambda = \begin{bmatrix} \Lambda_1 & 0 \\ 0 & \Lambda_2 \end{bmatrix}$$

where W_1 contains the first n eigenvectors, corresponding to the largest eigenvalues (Λ_1), defining the active subspace and W_2 contains the remaining eigenvectors, associated with small eigenvalues (Λ_2), defining the inactive subspace.

We choose n such that:

$$\sum_{i=1}^n \lambda_i \gg \sum_{i=n+1}^m \lambda_i$$

so that most of the function's variability is captured in the first n directions.

New active variables y and inactive variables z are defined:

$$y = W_1^T x, \quad z = W_2^T x$$

The function can now be rewritten as:

$$f(x) \approx g(y), \quad \text{where } g(y) = \mathbb{E}[f(x)|y]$$

This means that instead of working with m variables, the work now is done with only n active variables.

Since $f(x)$ is nearly constant in the z -directions, it is approximated using a response surface in the reduced space y (i.e., regression or interpolation):

$$f(x) \approx g(y) = \sum_{i=1}^n \alpha_i \phi_i(y)$$

where $\phi_i(y)$ are basis functions (e.g., polynomials, splines, or Gaussian processes) and α_i are coefficients determined from regression.

In the SBI platform, the eigenvalues and eigenvectors of the posterior distributions are computed. The eigendecomposition of the covariance matrix provides insight into how variations in different parameters influence the model output.

The computed matrix is:

$$M = \mathbb{E}_{p(\theta|x_o)} [\nabla_\theta p(\theta|x_o)^T \nabla_\theta p(\theta|x_o)]$$

where:

- θ represents the model's parameters;
- x_o is a specific observation of the model's output;
- $p(\theta|x_o)$ is the posterior distribution of parameters θ given the observation x_o (obtained through Bayes' theorem with SBI SNPE);

- M is the covariance matrix of gradients, computed as an expectation over the posterior distribution according to the Active Subspace method.

The eigenvalues and eigenvectors are then obtained through an eigendecomposition:

$$M = Q\Lambda Q^{-1}$$

where:

- Q is an $m \times m$ orthogonal matrix whose columns are the eigenvectors w_1, \dots, w_m ;
- Λ is a diagonal matrix with eigenvalues $\lambda_1, \lambda_2, \dots, \lambda_m$.

A strong eigenvalue means that the gradient of the posterior density is large: this is equivalent to saying that the output is sensitive to changes along the direction of the corresponding eigenvector.

1.6 Research goal

This research is part of a broader project focused on modeling brain activity in epilepsy patients undergoing DBS treatment. The project consists of two parallel research lines: one focused on patients undergoing DBS with simultaneous EEG recordings, and another based on scalp and iEEG data from epileptic patients when the DBS is switched off. Both research lines utilize EEG datasets collected at Medisch Spectrum Twente (MST).

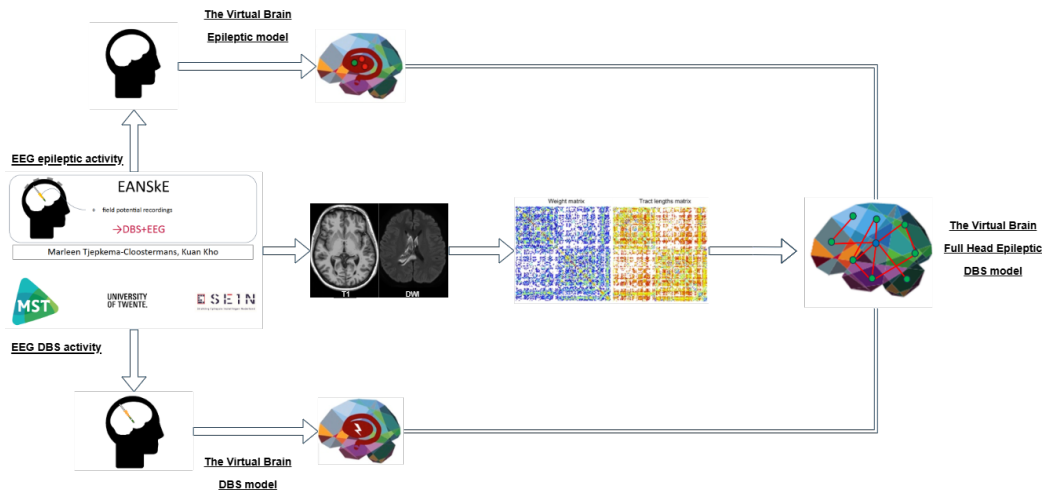


Figure 1.8: Overview of the broader computational project with two parallel research lines: one focused on patients undergoing DBS with simultaneous EEG recordings, and another based on scalp and iEEG data from epileptic patients when the DBS is switched off

Each branch develops its computational model: the DBS + EEG model integrates field potential recordings from implanted electrodes, while the EEG-only model focuses on intrinsic epileptic activity. The models are intended to be constructed using patient-specific brain connectivity matrices derived from T1-weighted and Diffusion-Weighted Imaging (DWI) MRI scans, which are processed

to generate weight and tract length matrices.

The ultimate goal is to integrate these two models into a unified whole-brain network model that includes both intrinsic and stimulation-driven dynamics. This approach allows for a patient-specific, data-driven framework tailored to individual brain connectivity. The final objective is to enhance personalized treatment strategies for epilepsy, leveraging neurostimulation and computational modeling to optimize therapeutic outcomes.

In this thesis, we focus on the EEG + DBS branch. Specific goals are model validation by sanity check within TVB, generation of evoked potentials in simulated EEG signal, comparison of the generated signal with the clinical data available, and finally followed by a sensitivity study on the primary parameters of the Jansen and Rit model.

Materials and method

An overview of the project phases is illustrated in Figure 2.1.

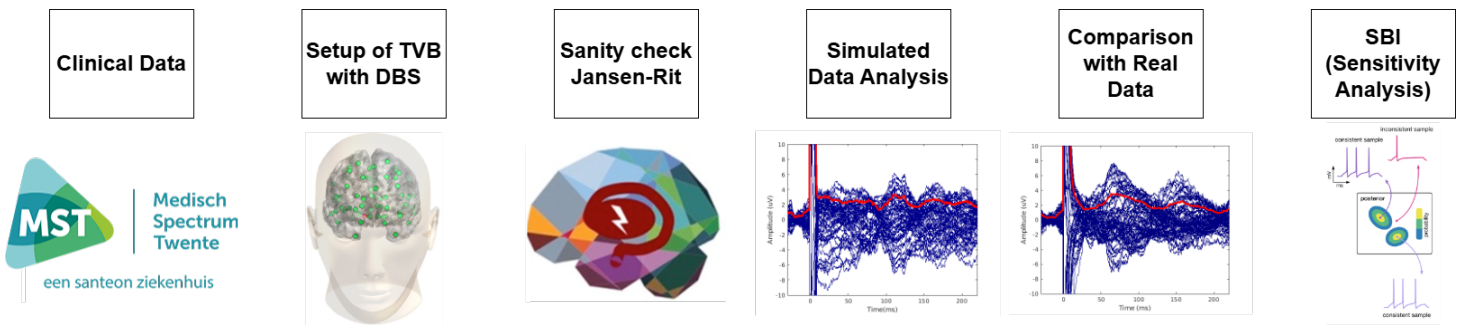


Figure 2.1: Overview of the project phases: introduction of available clinical data from the EANSkE study, description of the computational setup of TVB with DBS, sanity check of the Jansen-Rit model, analysis of simulated data, comparison with clinical EEG data, and concluding with sensitivity analysis using SBI

2.1 Clinical Data

In this research, we used data from the EANSkE study, which focuses on understanding the effects of DBS in patients with refractory epilepsy.

The main aim of the EANSkE study is to identify biomarkers from iEEG

recordings via DBS electrodes. By analyzing these biomarkers, the hope is to gain insight into how DBS affects brain dynamics and treatment response in epileptic patients.

In exploring this, the EANSkE study employs network analysis to assess structural and functional brain changes. Specifically, it hypothesizes that the analysis of both structural (i.e., resting-state fMRI) and functional (i.e., EEG and iEEG) brain data may reveal critical disruptions in neural activity in patients undergoing DBS.

The study follows a structured data collection protocol that involves 20 patients at MST. Data are collected at four distinct periods:

- baseline: before DBS implantation;
- immediate postoperative: 1 or 2 days after surgery;
- 12-month follow-up: one year after DBS implantation;
- 24-month follow-up: two years after DBS implantation.

For the data to comprehensively assess the neural dynamics, the acquisition included multiple data modalities: 64-channel EEG, 8-channel iEEG and Electrocardiogram (ECG) recordings. Furthermore, anatomical, fMRI and Diffusion-Tensor Imaging (DTI) scans were taken at baseline and 12 months postoperatively. In addition, patients complete four psychological well-being questionnaires at baseline, 12 months, and 24 months after surgery. Figure 2.2 provides an overview of the measurement setup, illustrating the data acquisition timeline.

In this thesis, we used the EEG recording *s0000820a* of patient DBS007 from the EANSkE study. The actual DBS pulse follows a biphasic, passive charge-balanced design, as illustrated in Figure 2.3. The pulse amplitude can reach up to

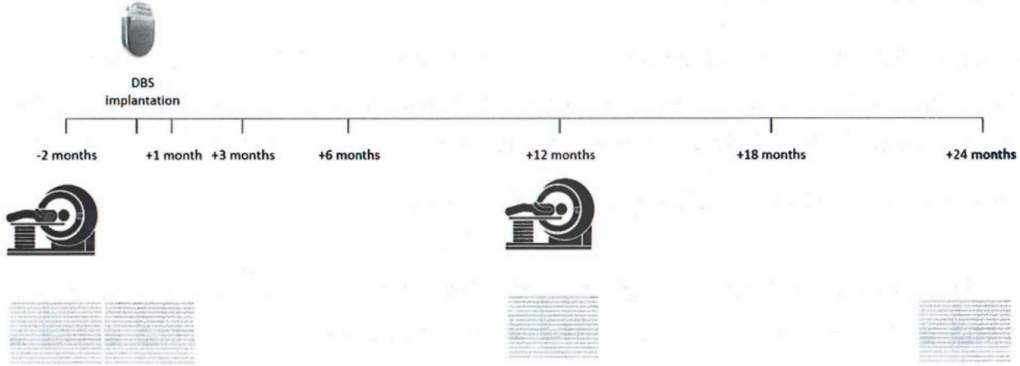


Figure 2.2: Overview of the measurement setup: MRI scans are made 2 months prior and 12 months after DBS implantation. Four EEG measurements are done: a baseline measurement, one day postoperatively, and at 12 and 24 months [Loosveld, 2024]

6 mA. While the pulse duration typically falls within the range of 60 to 90 microseconds. Stimulation frequency in the study is 4Hz alternating between hemispheres.

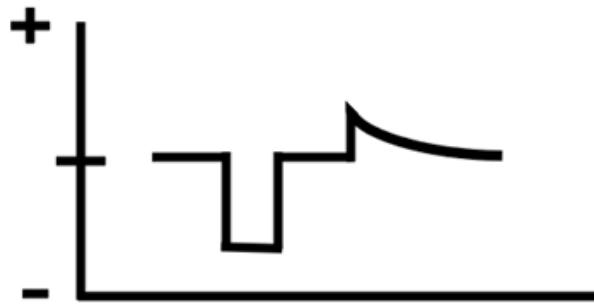


Figure 2.3: Biphasic passive charge-balanced DBS pulse as used for the data acquisition, trend is performed with each stimulation pulse followed by a charge recovery pulse, with the main aim of ensuring a net-zero charge deposition in the surrounding tissue

2.2 Setup of TVB with DBS

We generated simulated EPs within TVB due to DBS stimulation. The setup of TVB with DBS involved a structured process to integrate stimulation into the model. The configuration followed these steps:

- uploading of the connectivity matrix based on TVB’s default parcellation;
- selection of the stimulation node (right amygdala) within the network;
- application of a stimulation function with a predefined waveform and the possibility of adjusting the strength of the stimulation applied to the node through a weight from 0 to 1;
- execution of the simulation, where stimulation effects were propagated through the network via anatomical connections.
- projection of nodes activity to EEG sensors through the forward solution;

2.2.1 Nodes

To simulate EPs within TVB, we initialized a model using the dataset’s default 76-node connectivity matrix available in the .zip folder that was downloaded with the TVB software. In this setup, only one node received stimulation. The remaining nodes followed the standard NMM dynamics. These nodes interacted via the predefined connectivity matrix and received indirect stimulation through volume conduction from other nodes. Figure 2.4 illustrates the configuration of the full head model created within TVB and shows the stimulating node (red) against the other ones (green).

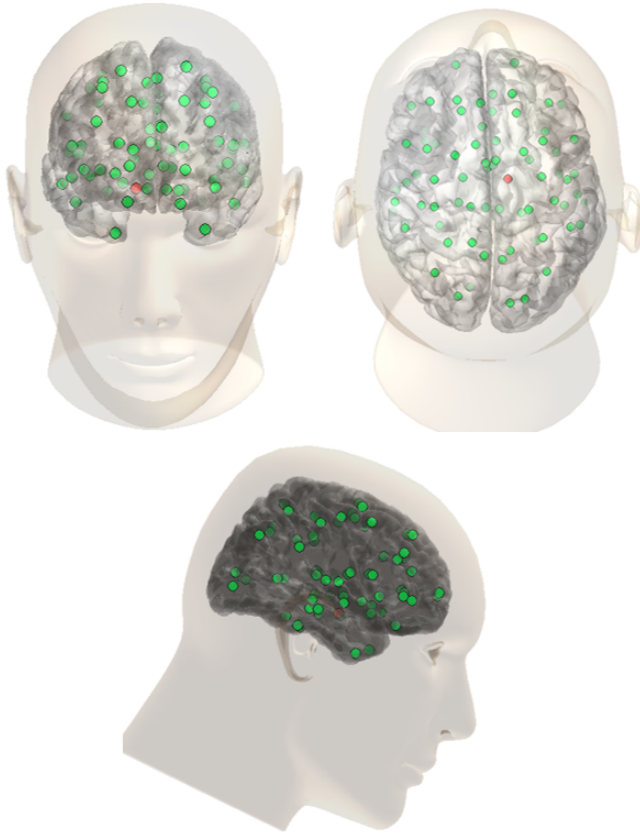


Figure 2.4: Frontal, lateral and upper view of the setup of TVB with DBS; in red the stimulation node (right amygdala), in green all the other nodes

The ANT was initially considered as the stimulation target due to its clinical relevance in epilepsy treatment. However, processing limitations with MRI data prevented the creation of a personalized connectivity matrix, and within TVB's default connectivity matrix, it was not possible to directly select a thalamic node connected to the other areas of the matrix. As a result, the right amygdala, another subcortical region, was chosen as the stimulation site. Unlike the ANT, the right amygdala is included in TVB's default parcellation and is interconnected, making

it a feasible alternative for the setup of TVB with DBS.

To ensure a balance between deterministic dynamics and stochastic variability, we made use of the Heun Stochastic integrator (<https://docs.thevirtualbrain.org/api/tvb.simulator.integrators.html>), which incorporates stochasticity into the model. Using an integration step size dt of 0.25, the simulation sampling rate was set to 4 kHz, ensuring consistency with the original data recordings. Furthermore, we chose a stimulation strength applied to the node of 1 (maximum), which allowed us to fully observe the effects of DBS on network dynamics.

2.2.2 Connectivity

The activity (state variables) that have been propagated over the long-range connectivity passes through the predefined coupling function before entering the equations of the model describing the local dynamics. The state variable vector for the k -th node or region in the network can be expressed as:

$$\text{derivative} = \text{noise} + \text{local dynamics} + \text{coupling}$$

where the coupling term is the time delays (thephysionet.org).

In our case, the coupling function between nodes is sigmoidal as described in the Jansen and Rit model (Eq. 1.3), of the following form:

$$c_{\min} + \frac{(c_{\max} - c_{\min})}{1.0 + \exp\left(-r \frac{(x-\text{midpoint})}{\sigma}\right)}$$

Each brain region (node), except for the stimulated one, was initialized with default parameter values. To enhance biological realism, noise was added only to the population of excitatory interneurons, following the differential equations of the original Jansen-Rit model, specifically Eqs. 1.6 and 1.7.

2.2.3 Projection matrix

In TVB, "monitors" (<https://docs.thevirtualbrain.org/api/tvb.simulator.monitors.html>) play a crucial role in recording significant values from simulations. These monitors capture and store the output data, allowing for analysis and interpretation of neural activity.

The most fundamental type of monitor is the Raw monitor, which records all simulated data without any transformation. It collects all state variables and modes from the model, all nodes of a region or surface-based simulation, and all integration time steps. This provides a comprehensive, unprocessed dataset that reflects the full scope of the simulation.

More advanced monitors go beyond raw data collection by incorporating physically realistic measurement processes. A key example is the EEG monitor, which simulates electroencephalography signals. This monitor applies a Forward solution using a precomputed lead field matrix to transform neural activity into an EEG signal, making the simulation results more comparable to real-world EEG recordings.

By offering both raw data collection and physiologically informed measurements, TVB monitors provide flexible and powerful tools for analyzing simulated brain dynamics.

2.3 Jansen-Rit sanity check

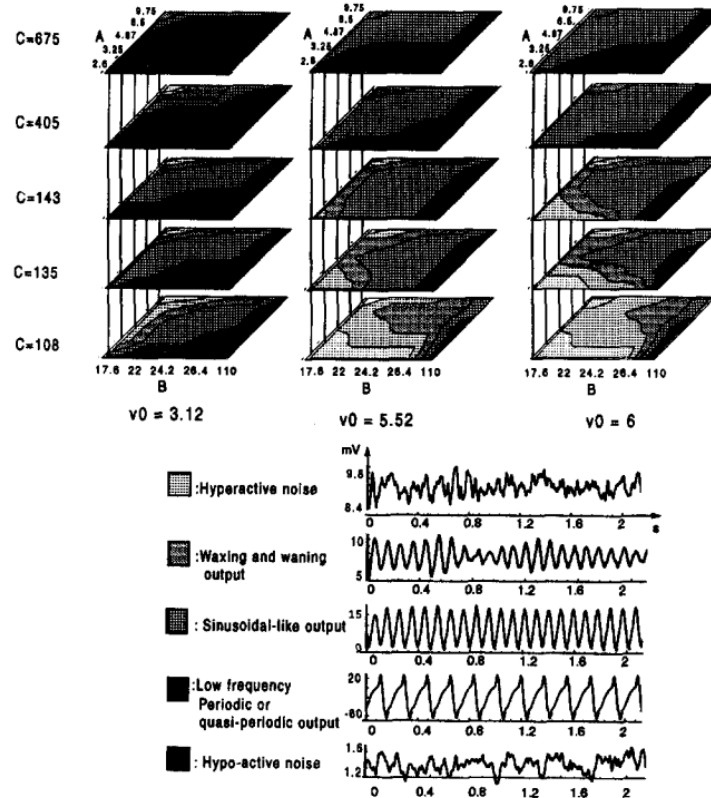


Figure 2.5: Exploration of the four-dimensional parameter-space for one column Jansen-Rit model with different activity types that arise. The input is random noise [Jansen and Rit, 1995]

To ensure the validity of our computational model, we conducted a sanity check based on the original Jansen-Rit NMM exploration (Figure 2.5). In their paper [Jansen and Rit, 1995] when explaining the functioning of their NMM, Jansen and Rit performed a multi-parametric exploration on four key parameters, A , B , v_0 and C , to analyze how different values influenced the resulting EEG activity. Their

study mapped out distinct regions of activity patterns in a single-column block model by varying these parameters.

The original study identified two primary noise regions in EEG activity trends. The results demonstrated that EEG activity followed a structured variation trend, with two dominant noise regions:

- Hypo-active noise: occurred when B was high relative to A (low excitatory feedback);
- Hyperactive noise: occurred when A was high relative to B (high excitatory feedback).

The experiment was also extended to a double-column model, revealing similar trends. Despite the increased complexity of parameter exploration in a two-column setup, the fundamental types of EEG activity and their trends remained consistent with the single-column results.

To verify these findings within our computational framework, we adapted a function designed to replicate the experiment in the double-column model. The function, sourced from file-jr95-py and designed for verifying the expected dynamics, was modified to accommodate the limitations of TVB in directly replicating the original model. Our goal was to reproduce the parameter-dependent behaviour observed in the original Jansen-Rit experiments. This step, if successful, will ensure that the model preserves its characteristic oscillatory behaviour despite structural differences between TVB's framework and the original model formulation.

However, we encountered specific differences between TVB and the original Jansen-Rit implementation:

- Noise distribution: the original model used uniformly distributed noise, while TVB employs a stochastic differential equation approach with normally distributed, additive noise;

- Model structure: the double-column structure in the original model includes additional PSP blocks for each connection, TVB replaces these with delay functions and a sigmoidal coupling function, altering the exact network response.

Although the two configurations are not identical but only similar, and so by comparing them we can only really reproduce the results of the paper with a uniform distribution, we will attempt to verify that the expected activity patterns could still be replicated under the right conditions, particularly by adjusting the global connectivity parameter C expressed in the code as $J * a_1 = C$.

We systematically increased the connectivity parameter to observe the transitions between different oscillatory states, mirroring the multi-parametric exploration conducted.

By reproducing this behaviour within TVB, we aim to confirm that our model accurately captures the core dynamics of the Jansen-Rit framework.

2.4 TVB simulation

After generating the output model, the final step involved deriving the simulated EEG signal by computing the difference between excitatory and inhibitory PSPs:

$$y(t) = y_1(t) - y_0(t) \quad (2.1)$$

where:

- $y_1(t)$ represents the excitatory post-synaptic potential (EPSP);
- $y_0(t)$ represents the inhibitory post-synaptic potential (IPSP).

This subtraction reflects the net cortical output $y(t)$, corresponding to the model's observable EEG activity.

2.4.1 Artifact

To simulate realistic DBS within TVB, we developed a custom stimulation function. This function mimics the stimulation delivered by Medtronic Model 3389 leads, which are connected to a Medtronic Percept PC Neurostimulator equipped with BrainSense technology. The custom function integrates DBS into TVB's multiscale NMMs by aligning with the framework's pre-existing functions. Designed with flexibility in mind, the function follows a specific mathematical formulation and allows users to freely adjust stimulation parameters, ensuring adaptability to different setups.

The custom stimulation function created to simulate realistic DBS is based on a three-phase waveform, the same one already seen in the real DBS in Figure 2.3. The function consists of:

- A negative rectangular pulse (stimulation phase);
- A short interphase interval (zero activity);
- A decaying exponential function (charge recovery phase).

The three phases of the function were mathematically defined as:

$$f(t) = \begin{cases} -a, & \text{if } \epsilon \bmod T < \tau \text{ and } \epsilon > 0 \\ a_{\exp} \cdot e^{-\frac{(\epsilon-x) \bmod T}{\tau_{\text{decay}}}}, & \text{if } x \leq \epsilon \bmod T < T \text{ and } \epsilon > 0 \\ 0, & \text{otherwise} \end{cases} \quad (2.2)$$

where:

- a is the amplitude of the negative rectangular pulse;
- $x = \tau + c$, where τ is the pulse duration, and c is the delay between the stimulation pulse and the charge recovery phase;
- $\epsilon = t - \text{onset}$, where *onset* is the stimulation start time;
- a_{\exp} is the amplitude of the decaying exponential recovery phase;
- τ_{decay} is the decay time constant.

Unlike extrinsic input current models, the virtual DBS setup did not directly stimulate the right amygdala. Instead, stimulation influenced the intrinsic neural activity of the right amygdala, which in turn affected the global network through the connectivity matrix. This indirect effect is evident in the discrepancy between the applied stimulation parameters (Figure 2.3) and the resulting neural activity in the simulated node (Figure 2.6).

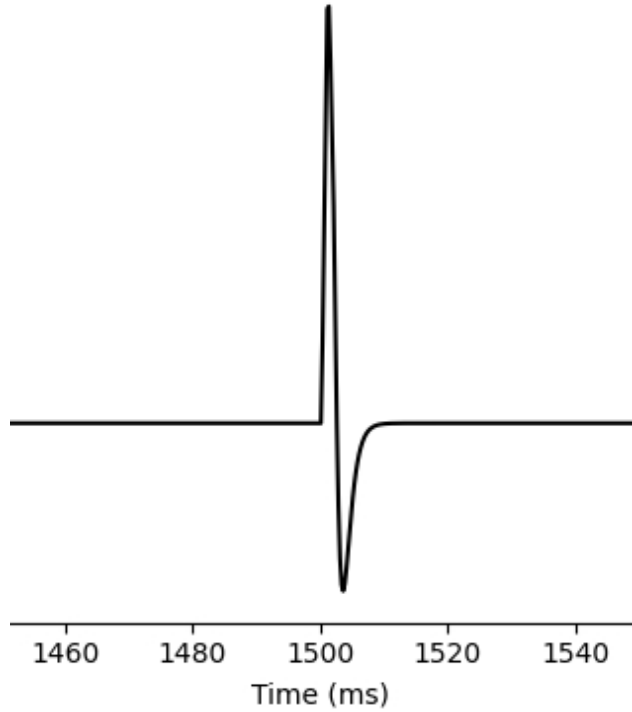


Figure 2.6: Visualization of a single DBS trial on Jansen-Rit right amygdala, the inverse sign of the stimulation to the actual one depends on electrode polarization

Since the stimulation modulated intrinsic neural activity, adjustments were necessary to match realistic DBS-induced neural responses observed in experimental studies. Final stimulation settings were determined iteratively, guided by simulation outcomes. The goal was to match the network-wide oscillatory response seen in clinical DBS studies. Although the real stimulation protocol applied a bilateral alternating hemisphere 4 Hz stimulation (such that each hemisphere received 2 Hz), TVB's constraints required us to model it as a single-hemisphere 2 Hz stimulation.

All parameter tuning was conducted to achieve optimal alignment between

simulated and experimental data, refining the model to better reflect realistic DBS effects on brain dynamics.

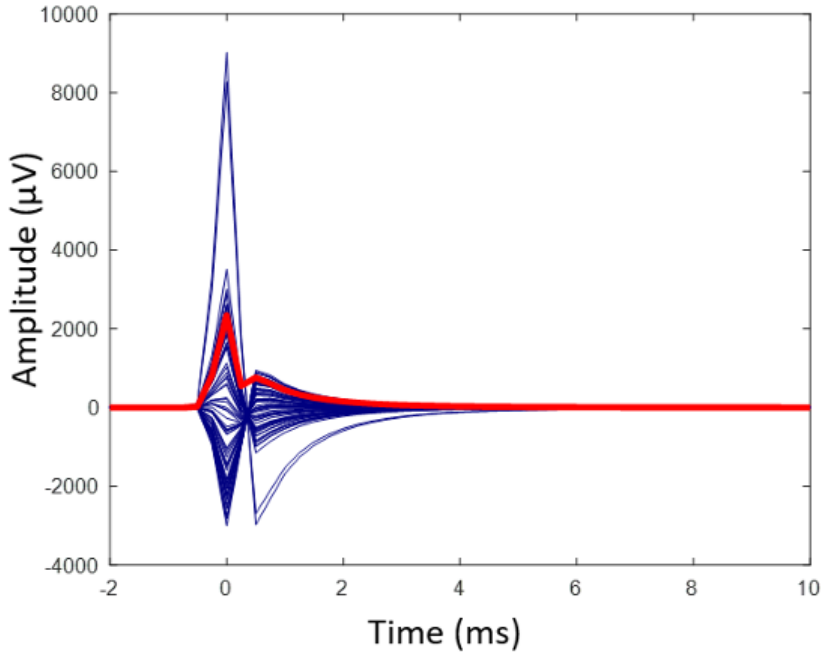


Figure 2.7: Averaged EEG Global Mean Field Power around peak events after high-frequency DBS, each blue line represents an individual channel's signal, while the red line denotes the absolute average across all electrodes [Loosveld, 2024]

The artifact modeling process was guided by real stimulation artifacts observed in experimental data. The stimulation artifact used as a reference for designing the simulated artifact in TVB is shown in Figure 2.7.

In real data, stimulation artifacts arise from multiple sources (also visible from Figure 1.1, including:

- Electromagnetic interference caused by high-frequency pulses;
- Volume conduction effects within surrounding neural tissue;

- Harmonic distortions and filtering effects due to electrode properties.

However, TVB does not directly model electrical fields. As a result, the simulated artifact does not emerge from direct electromagnetic interference but instead from the propagation of neural activity through anatomical connections. This difference required parameter adjustments to make the simulated artifact resemble real-world observations.

To refine the artifact simulation and control its propagation, two modifications were made. First, the stimulation channel was influenced by the intrinsic activity of the NMM, causing the artifact to propagate through volume conduction rather than appearing as an isolated stimulation effect. To minimize unintended propagation effects, we implemented a deterministic integrator by setting the noise level to zero across all neural populations at the stimulation source node. This adjustment suppressed the influence of the node’s intrinsic activity, ensuring that the response was driven exclusively by the applied stimulation parameters.

Despite these modifications, the artifact still displayed an unexpected temporal deformation, causing it to persist abnormally over time. To resolve this issue, we fine-tuned the node parameters a and b to align the temporal duration of the stimulation with its expected physiological timescale. The new values are shown in Table 2.1.

Parameter	Std Value	New Value
a	0.1	4.5
b	0.05	3.5

Table 2.1: Set of fine-tuned values for the model parameters to align the temporal artifact duration of the stimulation with its expected physiological timescale

These refinements ensured that the simulated artifact closely matched real DBS-induced artifacts while maintaining biological plausibility. The connectivity matrix remained unchanged, with all other nodes using the same Jansen-Rit model parameters. This setup allowed a realistic representation of stimulation-induced artifacts.

2.4.2 Evoked Potentials

To generate evoked responses within TVB, the current parametric configuration incorporates previously described modifications. Table 2.2 below presents the key model parameters, distinguishing between generic node values and the fine-tuned parameters applied to the stimulated region, the right amygdala.

Parameter	Generic Node Parameters	Amygdala Parameters
A	3.25	3.25
B	22.0	22.0
a	0.1	4.5
b	0.05	3.5

Table 2.2: Set of values for the model parameters on the generic node and of the fine-tuned parameters for the stimulation node (right amygdala)

The evoked responses within TVB are generated based on a parameter configuration that balances standard values with fine-tuned modifications for stimulation. The model setup ensures consistency with theoretical foundations while adapting to the specific dynamics of the stimulated region.

The parameters of the generic node were chosen to align with standard values established both in TVB and in the original Jansen-Rit model. These values

represent a well-validated baseline for simulating cortical activity and provide a reference for modifications applied to specific regions. The right amygdala, as the designated stimulation node, required parameter adjustments to better capture its distinct neural properties.

In addition to these parameters, the noise value is set to 1.0, maintaining consistency with the previous modifications.

The simulation operates with a monitor sampling interval of 0.25 ms, aligning precisely with the integrator frequency of 4 kHz.

The total duration of the simulation spans 120k samples, corresponding to 30 seconds (30k ms). For analysis, the trial window surrounding the stimulation peak is defined as 250 ms, providing a sufficient temporal range to capture the onset, peak, and decay of the evoked responses.

2.5 Qualitative comparison with clinical EEG

After generating the simulated EEG signals in TVB, the data was post-processed. The simulated signals were saved as a NumPy (.npy) file and subsequently imported into MATLAB using the npy-matlab code <https://github.com/kwikteam/npy-matlab>. Once loaded, the data was analyzed using FieldTrip [Oostenveld *et al.*, 2011], a software toolbox for EEG and MEG data analysis.

To analyze stimulation-related activity, the data was epoched and processed using FieldTrip functions. Epoching was performed using *ft_timelockanalysis* which computed trial-averaged responses based on predefined stimulation instants within a time window of 30 ms before to 220 ms after stimulation. The processed signals were then analyzed using the following steps:

- Global Mean Field Power (GMFP) computation: computed using *ft_globalmeanfield* whose formula is

$$GMFP(t) = \sqrt{\frac{\sum_{i=1}^K (V_i(t) - V_{\text{mean}}(t))^2}{K}}$$

to evaluate signal strength across electrodes;

- Topographic Mapping (Topoplots) computation: visualized using *ft_topoplotER* to observe spatial EEG distributions.

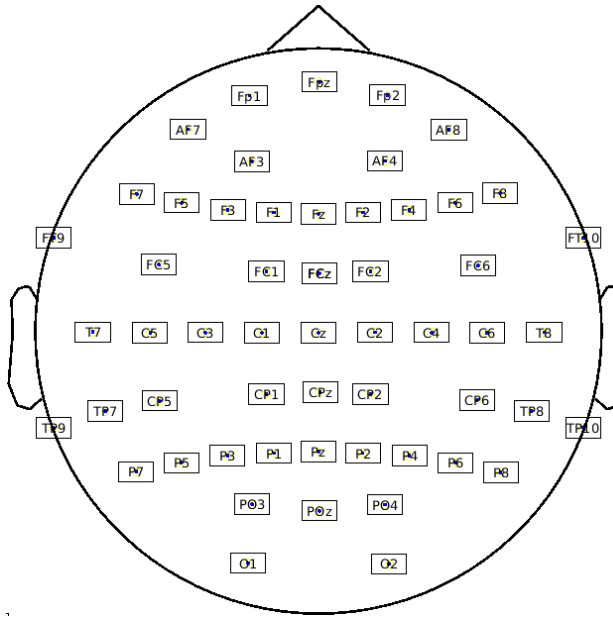


Figure 2.8: Personalized EEG cap, the configuration merged elements from both EANSkE and TVB EEG sensors, ensuring the best possible electrode correspondence

Since the standard TVB EEG sensor configuration did not align with the 10/20 system used in the EANSkE project, a customized cap layout was created, visible in Figure 2.8. The new configuration merged elements from both systems, ensuring the best possible electrode correspondence by:

- Removing electrodes not present in both configurations;

- Retaining electrodes that matched between the two systems;
- Approximating missing electrodes using the closest available channels.

The final configuration consisted of 56 sensors, with specific approximations made for some signals:

- FT7 and FT8 signals were approximated using FT9 and FT10;
- PO7 and PO8 signals were approximated using TP9 and TP10.

These approximations were deemed acceptable for the study's objectives. In addition to adjusting electrode labels in the topoplots, the corresponding signals were correctly assigned in MATLAB before processing. This ensured that the simulated EEG signals were accurately extracted from their sources, leading to reliable and interpretable visualizations in the final plots.

To evaluate the accuracy of the simulated data, we compared it to real EEG recordings from the EANSkE project dataset. Specifically, we analyzed the DBS-EEG dataset of patient DBS007, which contained several DBS stimulation protocols. We selected the protocol most relevant to our study, single-hemisphere 2 Hz stimulation, which in reality corresponds to a bilateral alternating 4 Hz stimulation applied in the two hemispheres.

To ensure consistency between real and simulated data, we applied the same analysis pipeline to the EEG recordings. Following the approach of [Loosveld, 2024], we processed the real EEG signal using FieldTrip functions, replicating the same steps used for simulated data: computation of GMFPs to assess overall EEG signal strength and topoplots to visualize spatial activity distribution.

After processing, we conducted a qualitative comparison between the real and simulated signals. We analyzed their different GMFP and topographic representations to assess how well the simulation replicated real DBS-induced EEG dynamics.

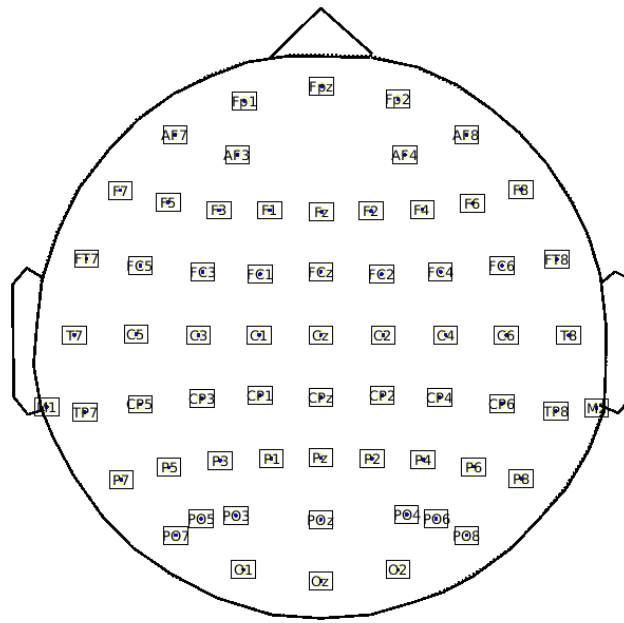


Figure 2.9: Real EEG cap, from clinical data [Loosveld, 2024]

This comparison provided insights into the effectiveness of the simulation model, allowing us to evaluate its ability to capture relevant neural responses.

2.6 Sensitivity analysis

For our sensitivity analysis, we considered two simulation settings:

- 10k simulations performed, extracting 100k samples for the posteriors plot distributions;
- 100k simulations performed, extracting 1 million samples for the posteriors plot distributions.

Since our focus was on evaluating parameter influence, we applied the Active Subspace method previously explained only up to the eigendecomposition step and omitted the projection onto the active subspace, as this was unnecessary for our specific objectives.

Results

3.1 Jansen-Rit sanity check

The first observed state was the hyperactive noise regime, characterized by excessive excitatory feedback. This is observable in Figure 3.1, where the model exhibits sustained high-amplitude fluctuations.

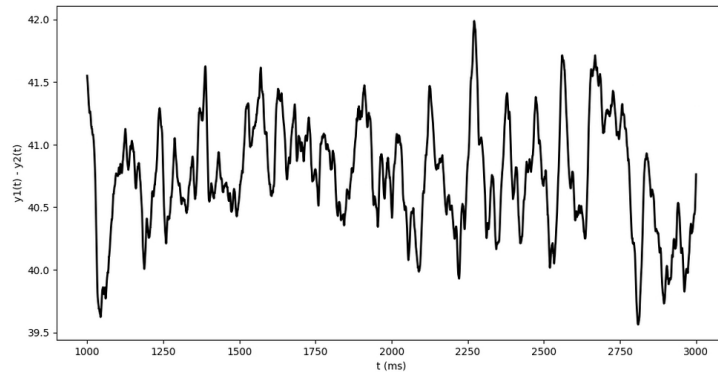


Figure 3.1: Jansen and Rit model sanity check, Hyperactive noise activity, sustained high-amplitude fluctuations

As the connectivity values were modified, the system transitioned into a waxing and waning oscillatory state, characterized by intermittent bursts of activity, as

seen in Figure 3.2.

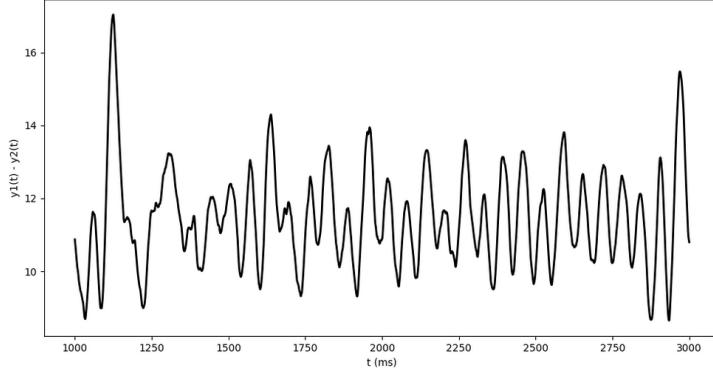


Figure 3.2: Jansen and Rit model sanity check, Waxing and waning activity, characterized by intermittent bursts of activity

The core behaviour of the Jansen-Rit model is its ability to produce alpha-band oscillations, a key feature of cortical activity. This sinusoidal-like output is successfully reproduced in Figure 3.3, demonstrating that the adaptation within TVB maintains this fundamental behaviour.

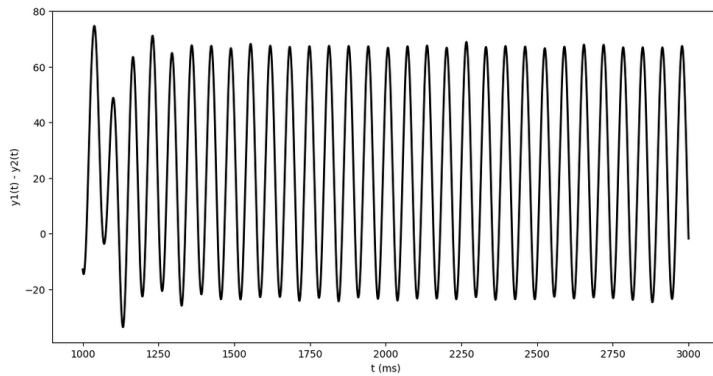


Figure 3.3: Jansen and Rit model sanity check, sinusoidal-like output

Further increasing the connectivity parameter led to a transition into a quasi-

periodic (low-frequency periodic) state, captured in Figure 3.4. This phase reflects a transition zone between regular oscillatory activity and more complex network dynamics.

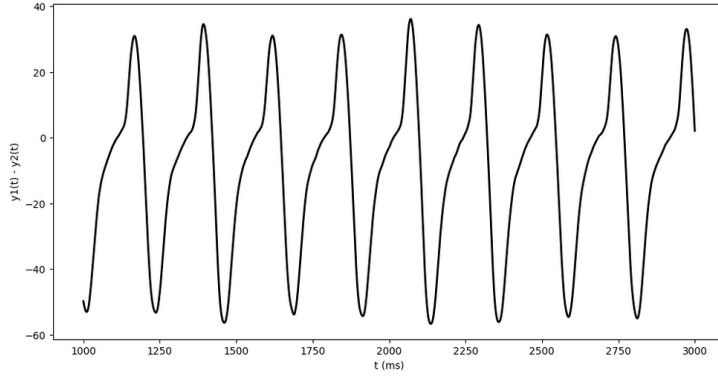


Figure 3.4: Jansen and Rit model sanity check, Quasi-periodic

Finally, as inhibitory feedback increased, the model entered the hypoactive noise regime, where activity became significantly suppressed. This corresponds to the second large noise region observed in the original Jansen-Rit framework, as illustrated in Figure 3.5.

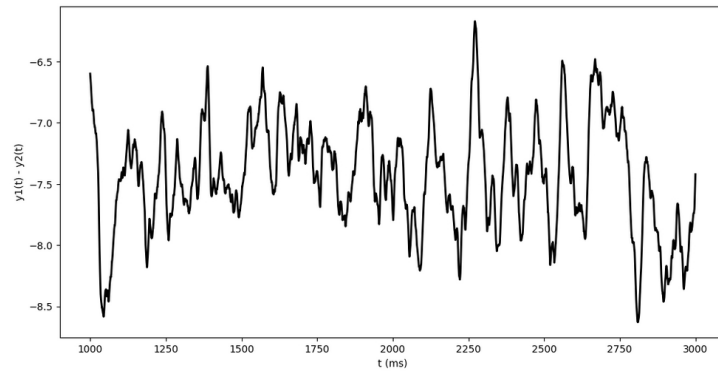


Figure 3.5: Jansen and Rit model sanity check, Hypo-active noise

These results confirm that our TVB implementation of the Jansen-Rit model successfully replicates its fundamental oscillatory dynamics, despite the differences in noise formulation and network structure. The key transitions between hyperactive noise, waxing and waning, alpha-band oscillations, quasi-periodic states, and hypoactive noise were all observed, verifying that the adaptation retains biologically meaningful behaviour.

3.2 Simulated data

To assess the validity of the simulated EEG signals, we processed the data by removing electrodes not present in the real configuration from EANSkE and epoching the signals around peak events. The preprocessing followed the methodology described in the previous section. To minimize epoching errors, the first and last peaks from every electrode were discarded.

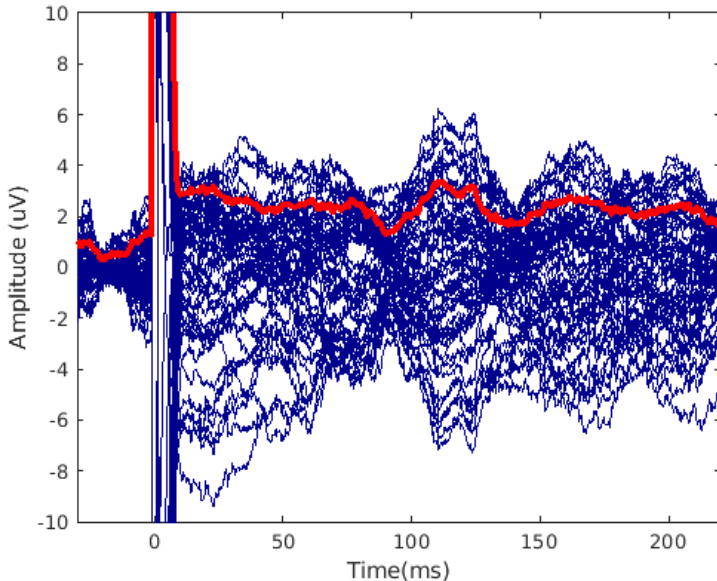


Figure 3.6: Simulated averaged signals around peak events; each blue line represents an individual channel's signal, while the red line denotes the GMFP

Figure 3.6 presents the averaged signal around peak events. In this visualization, each blue line represents an individual electrode's signal, while the red line denotes the absolute average across all electrodes. A prominent artifact is visible at 0 ms, where the signal magnitude is considerably larger than the sur-

rounding physiological activity. This artifact appears to be a direct consequence of DBS stimulation, introducing a transient electrical disturbance before the system stabilizes.

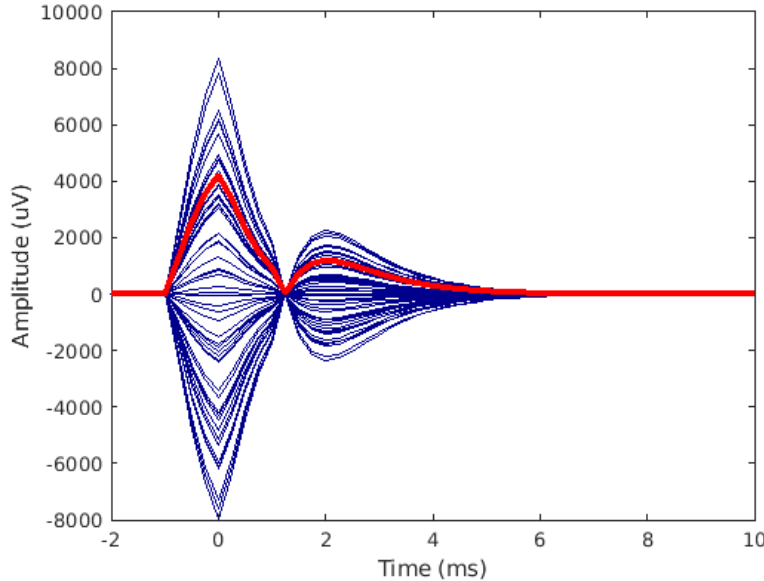


Figure 3.7: Simulated averaged signals around peak events artifact, each blue line represents an individual channel's signal, while the red line denotes the GMFP

To further analyze the artifact's structure, we examined its shape, temporal decay, and amplitude. Figure 3.7 isolates the artifact component, showing its distinct waveform characteristics.

The overall temporal activity patterns in the simulation exhibit strong qualitative similarities to real EEG recordings. This could indicate that the simulated signal is physiologically interpretable rather than an arbitrary computational construct.

The DBS-induced response appears to consist of three distinct evoked responses

occurring at approximately 25 ms, 110 ms, and 165 ms, as highlighted in Figure 3.6. These responses suggest a structured neurophysiological reaction to stimulation, further reinforcing the realism of the simulated data.

To understand how the artifact propagates across electrodes, we visualized its spatial distribution using a topoplot (Figure 3.8).

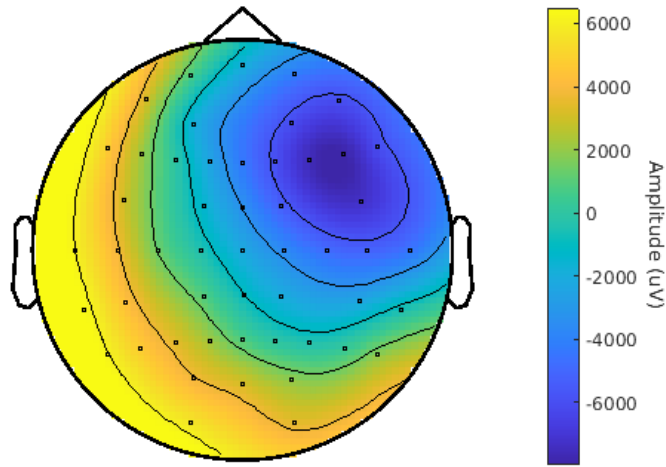


Figure 3.8: Spatial distribution of the simulated artifact

The artifact's topography aligns with expectations, displaying a strong negative response in the upper-right hemisphere, which matches the location of the stimulated node (as seen in Figure 2.4 from the previous section). This consistency indicates that the artifact follows a physiologically plausible propagation pattern rather than an interpolation artifact or numerical artifact.

Furthermore, apart from the stimulation-induced activity, the topoplot does not exhibit unusual patterns such as sharp discontinuities, excessive edge artifacts, or noise distortions. This suggests that the electrical distribution remains reliable, further supporting the physiological validity of the simulated data.

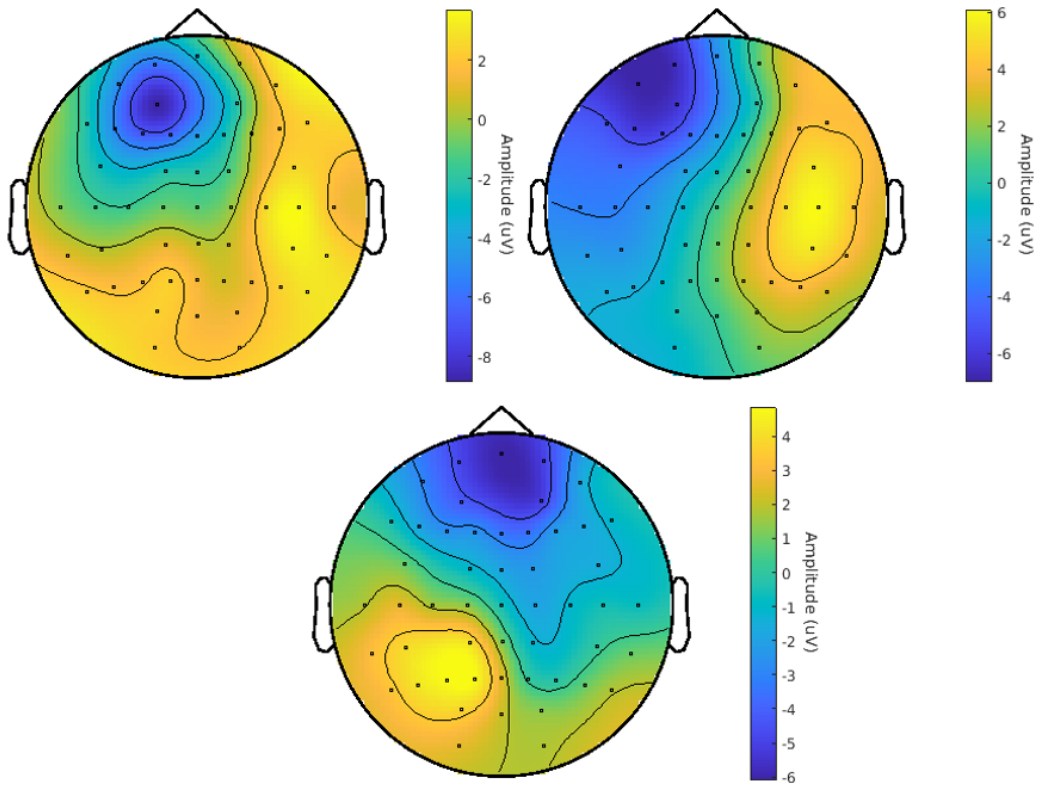


Figure 3.9: Spatial distribution of the simulated evoked responses at 25 (left), 110 (right) and 165 (middle) ms

Equivalent considerations concerning those just carried can be made for the topographies of the EPs, where the presumed responses at 25, 110 and 165 ms in Figure 3.9 assume a topographical distribution of the electrical activity that is qualitatively similar to the one relative to the spatial distribution of the artifact. The activity is non-noisy and free of unusual patterns, which would cast doubt on its physiological plausibility. This reinforces the credibility of the simulated signal's neurophysiological accuracy.

3.3 Qualitative comparison with real data

To evaluate the physiological plausibility of the simulated data, we performed a qualitative comparison against real EEG recordings obtained from the EANSkE project and the pipeline described in [Loosveld, 2024]. This comparison focuses on global signal characteristics, artifact morphology, and topographical distributions to determine whether the simulated signals exhibit realistic neural activity patterns.

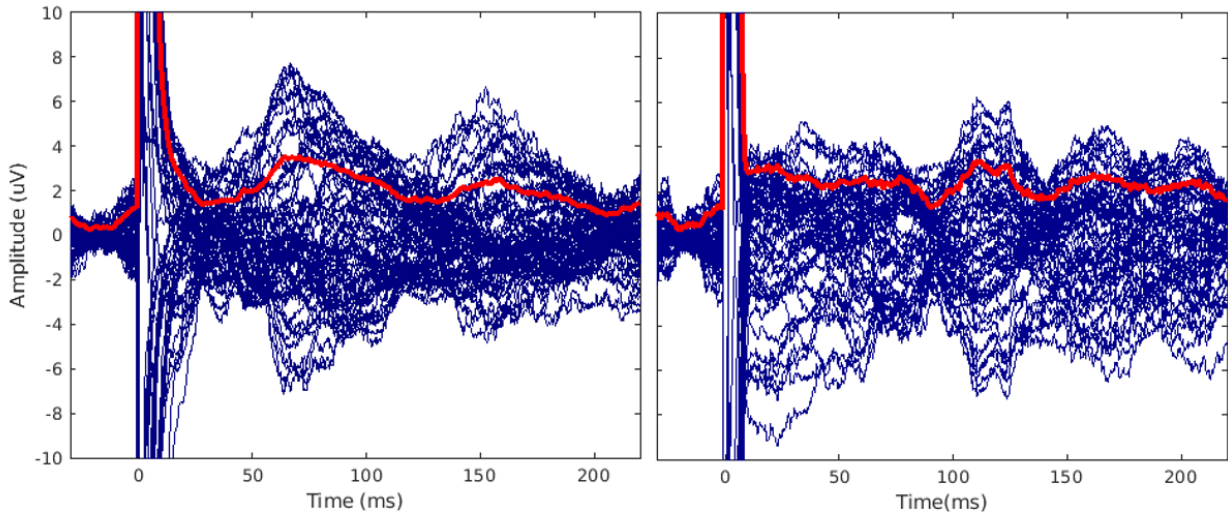


Figure 3.10: Comparison between averaged real (left) and simulated (right) signals around peak events, each blue line represents an individual channel's signal, while the red line denotes the GMFP

Figure 3.10 presents both the GMFP derived from real EEG data following DBS stimulation and the simulated GMFP. When compared, a strong resemblance is evident. The similarity in waveform shape and amplitude between the two signals supports our earlier hypothesis that the simulated data closely resembles real EEG recordings.

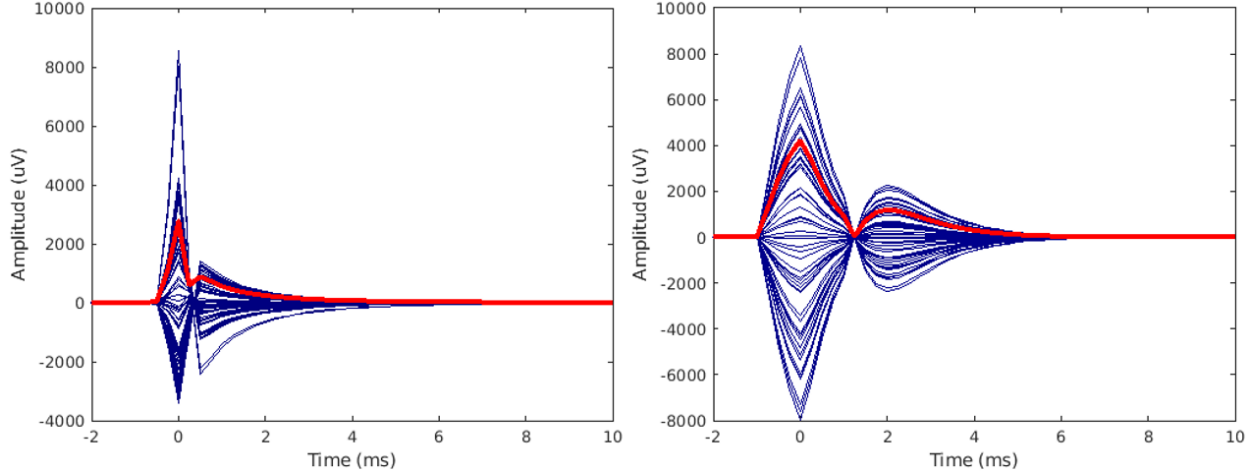


Figure 3.11: Comparison between averaged real (left) and simulated (right) signals around peak events artifact, each blue line represents an individual channel's signal, while the red line denotes the GMFP

A key feature in both the simulated and real data is the stimulation artifact, which appears as a prominent signal distortion immediately following the DBS pulse. Figure 3.11 compares the artifacts in the real and simulated EEG signals, highlighting their structural similarities. Both artifacts exhibit a clear verisimilitude in shape, characterized by:

- A sharp initial peak caused by the stimulation pulse;
- A subsequent repolarization rise;
- A gradual decay phase following stimulation onset.

However, minor discrepancies are noticeable:

- The simulated artifact has a slightly longer time course;
- The simulated artifact exhibits a slightly greater inferior amplitude.

Despite these differences, the overall artifact morphology aligns well between real and simulated data, reinforcing the validity of the model.

To further validate the simulation, we examined the topographical distribution of the stimulation artifact. The real and simulated artifact's spatial distribution is shown in Figure 3.12. A key anatomical distinction emerges:

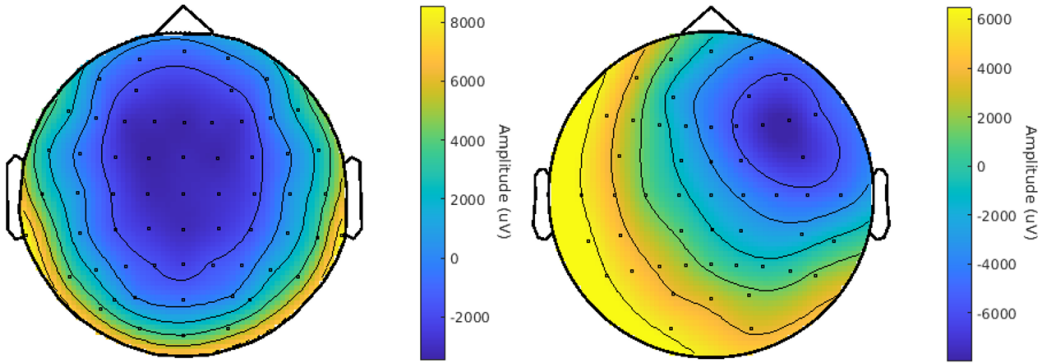


Figure 3.12: Spatial distribution of the real (left) and simulated (right) artifacts

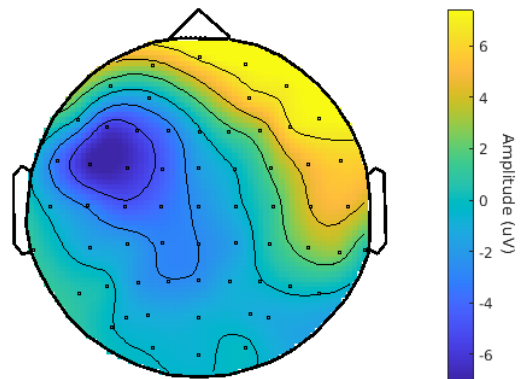
- In the simulated data, the artifact is right-lateralized, reflecting the location of the right amygdala as the stimulation site;
- In the real EEG data, the artifact is more centered, consistent with stimulation at the ANT.

Beyond artifacts, we also examined the evoked responses following DBS stimulation in both datasets. The real EEG topoplots for the evoked potentials at 63 ms and 157 ms are shown in Figures 3.13a and 3.13b, respectively.

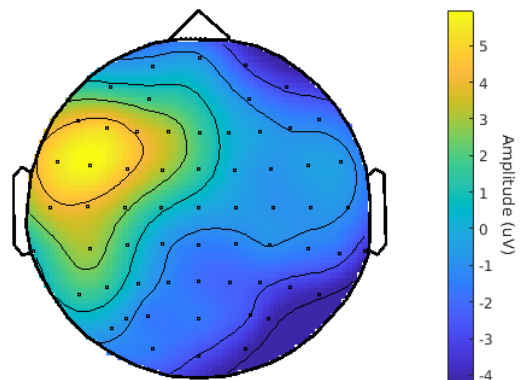
These real topographies exhibit striking similarities to the simulated topoplots at 25, 110, and 165 ms (Figures 3.9). Specifically:

- Both simulated and real evoked potentials exhibit clear dipole structures, suggesting a meaningful cortical response;

- No sharp discontinuities, edge artifacts, or interpolation errors were observed, further supporting signal integrity.



(a) Topoplott at 63 ms



(b) Topoplott at 157 ms

Figure 3.13: Topoplots of the two real evoked responses at 63 and 157 ms

Despite the strong similarities between the real and simulated signals, one important limitation must be addressed. The simulated data was generated using the amygdala as the stimulation target, whereas the real data reflects ANT stim-

ulation. While the amygdala serves as a reasonable subcortical proxy, it is not the ANT, meaning that fine-tuning model parameters to precisely match real EEG recordings is not feasible.

Parameter tuning via SBI cannot be applied, since the spatial discrepancy between the stimulation sites introduces unavoidable variability and although the amygdala produces physiologically plausible responses, they are not an exact match for ANT-evoked dynamics.

As a result, rather than parameter tuning, we will proceed with a sensitivity analysis to assess how variations in model parameters affect simulated network dynamics.

3.4 Sensitivity Analysis

To assess the influence of key parameters in the Jansen-Rit model, we performed a sensitivity analysis focusing on the four main parameters: (A, B, a, b) . The analysis aimed to quantify how variations in these parameters affect the GMFP, computed by averaging the mean trial across all available EEG electrodes in TVB. By conducting 10k and 100k simulations, we analyzed the posterior distributions of these parameters, identifying their relative importance and interdependencies through pairwise posterior distribution plots and eigendecomposition.

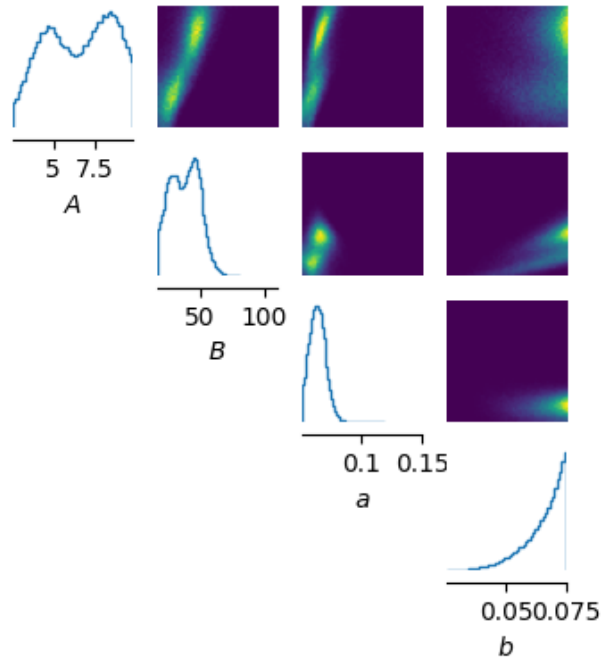


Figure 3.14: Sensitivity analysis posterior distributions of the four parameters after 10k simulations and the extraction of 100k samples

Figure 3.14 presents the posterior distributions of the four parameters after

10k simulations and the extraction of 100k samples.

- The diagonal elements display marginal distributions, highlighting the likelihood of each parameter;
- The off-diagonal elements show pairwise joint distributions, revealing relationships between parameters.
- A brighter density region in the joint posterior plots indicates a stronger correlation between parameters.

If two parameters are strongly correlated, their joint posterior (off-diagonal) will show an elongated or diagonal shape, while if they are independent, their posterior distribution will be more uniform.

The computed eigenvalues and eigenvectors are:

Eigenvalues:

$$\left[1.1455 \times 10^{-6}, \quad 1.9739 \times 10^{-6}, \quad 4.0743 \times 10^{-5}, \quad 3.4917 \times 10^{-4} \right]$$

Eigenvectors:

0.9161	0.2206	-0.0309	0.3335
0.2590	-0.2481	-0.7043	-0.6127
0.2571	0.0724	0.6709	-0.6918
0.1663	-0.9405	0.2302	0.1865

Regarding the 10k pairwise posterior distribution plot, we can see how the marginal distributions show:

- Parameter A exhibiting a bimodal distribution, suggesting two regions of high probability;
- Parameter B showing a greater likelihood for lower values;
- Parameter a displaying a sharp peak, indicating high certainty in the estimation;
- Parameter b presenting a strong preference for higher values, and a for lower ones.

In the joint distributions, A and B show a strong correlation through the elongated diagonal pattern, whereas other parameter pairs show a lower correlation or uniform distribution, indicating independence.

About eigendecomposition, as mentioned above, the largest eigenvalue (3.4917×10^{-4}) indicates the primary direction of variance in the parameter space, while small eigenvalues suggest a low influence on variability.

The fourth eigenvalue is the largest, so we are going to analyze the fourth eigenvector, or $[0.1663, -0.9405, 0.2302, 0.1865]$, from which we can see that the largest amount in absolute value is the second one, or B , while the other values are about the same. So, in this first case B is the most sensitive among the parameters.

If we follow the same reasoning for the second largest eigenvalue, (4.0743×10^{-5}) that is the third one, we analyze the third eigenvector $[0.2571, 0.0724, 0.6709, -0.6918]$ and we can see that, in absolute value, the fourth one, or b is the most sensitive among the parameters. It is worth noting that in this last case, also a has almost a similar value as b , implying that the two could be equally important.

To refine our understanding of parameter sensitivity, we increased the number of simulations to 100k, extracting 1 million samples. The resulting posterior distributions are shown in Figure 3.15.

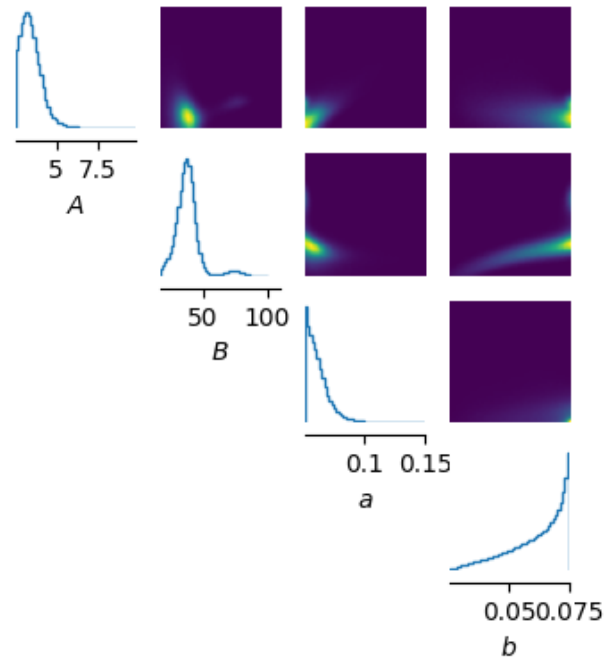


Figure 3.15: Sensitivity analysis posterior distributions of the four parameters after 100k simulations and the extraction of 1 million samples

Again, we show the respective eigenvalues and eigenvectors of the posterior distributions of the parameters obtained by the eigendecomposition:

Eigenvalues:

$$\left[2.5381 \times 10^{-6}, \quad 1.6100 \times 10^{-5}, \quad 2.2885 \times 10^{-5}, \quad 1.0073 \times 10^{-4} \right]$$

Eigenvectors:

0.0889	0.7045	0.6427	0.2877
0.0963	-0.2327	0.5865	-0.7698
0.4112	0.5922	-0.4838	-0.4961
0.9021	-0.3145	0.0947	0.2800

Concerning the 100k pairwise posterior distribution plot:

- The bimodal distribution of parameter A disappears, implying a refined posterior due to a larger sample size;
- Parameter B now shows a sharp peak, indicating higher convergence;
- Parameter a shows a sharper distribution, leaning towards the values of the left extreme;
- Parameter b maintains its nature despite showing an overall probability more distributed over the interval.

In the joint distributions, A and B still show a strong correlation, whereas other parameter pairs maintain the same lower correlation trend.

In this case, the largest eigenvalue is slightly lower than previously (1.0073×10^{-4} vs 3.4917×10^{-4}), and this could be a sign of a more balanced variance distribution between parameters, and this is further proven by the fact that the smallest eigenvalue is slightly larger (1.1455×10^{-6} vs 2.5381×10^{-6}).

The eigenvector associated with the largest eigenvalue is again the fourth one, or $[0.9021, -0.3145, 0.0947, 0.2800]$ and this shows how no longer parameter B is dominant, instead A is the one that contributes the most, even if in this case it is worth to be noted, concerning the previous protocol, how the contribute of the second biggest value in the eigenvector, or A , is bigger.

The change in eigenvectors indicates a shift in the principal variance directions that could be due to the increased sample size and/or the increased number of simulations.

Regarding the second largest eigenvalue, 2.2885×10^{-5} , that is the third one, we are going to look at the third eigenvector, or $[0.4112, 0.5922, -0.4838, -0.4961]$. We can see how the second value, or B is the biggest one. But it is important to observe, in this case, how all the other parameters have a high value, indicating that the four parameters have all their importance on the final output.

The swap in eigenvectors indicates a shift in the principal variance directions that could be due to different things, among which increased sample size and/or the increased number of simulations.

The increment in the number of samples shows more precise posterior distributions with sharper peaks and better parameter estimation. The eigenvalues are slightly reduced, and this is a sign that the variance is spread more evenly.

For the 10k protocol, we found out that the two most sensitive parameters were B and b . Instead, for the 100k protocol, we obtained that the two most sensitive parameters were A and B .

This sensitivity analysis highlights the complex dependencies between parameters in the Jansen-Rit model and provides valuable insights into their respective roles in shaping the simulated neural dynamics.

Discussion

4.1 Key findings

From our analyses, we have identified several important observations regarding the validity, neurophysiological relevance, and sensitivity of the Jansen-Rit model within our simulation framework.

The sanity check of the Jansen-Rit model confirmed its suitability for our investigative purposes. This demonstrates that, even in a complex computational model framework, the original activity types from Jansen and Rit's single cortical column can still emerge. Consequently, the model's ability to reproduce EPs would remain valid. The sanity check provides essential validation for the computational model, ensuring its reliability for further analysis. This consistency suggests that the model retains its fundamental properties, allowing for extensions to more complex network configurations without losing biological plausibility. All this was done knowing the limitations explained above within the TVB framework.

The analysis of the simulated signal using GMFP and topoplots provided further evidence that the model generates biologically meaningful neural activity. Key findings include:

- The simulated signal aligns with neurophysiological expectations, supporting

its potential for neuroscientific investigations;

- The presence of evoked responses at distinct time points (25, 110 and 165 ms) suggests that DBS elicits structured neural reactions, reinforcing the validity of the modeled neurophysiological processes;
- The topographies of the artifact and evoked potentials exhibit realistic spatial distributions, further strengthening confidence in the reliability of the simulated signal.

These topographies confirm that the electrical activity from the simulated EPs is reliable. The spatial distributions align with physiological expectations, reinforcing the validity of the simulation. The simulated EEG signal displays key characteristics that suggest it is a reasonable approximation of physiological neural activity:

- The artifact's spatial distribution aligns with the stimulation site, supporting realistic propagation of electrical activity;
- The EPs at 25, 110, and 165 ms exhibit stable, biologically plausible topographic distributions.

While these results do not prove that the simulated signal is a replica of real EEG activity, they strongly suggest that the simulation is not arbitrary. Instead, the neurophysiological properties embedded in the model appear to be preserved, making the dataset suitable for further analysis in DBS research and network-level investigations.

The parameter values in Table 2.2 provide an interesting basis for analysis. The fact that only a and b were modified to achieve a correct response to stimulation suggests that these parameters play a critical role in fine-tuning the system. This

adjustment may indicate the extent of correction required to produce the desired neural response.

The stability of A and B across all nodes is also noteworthy. Since these values remain unchanged, it suggests that the primary mechanisms governing excitatory and inhibitory interactions do not require modification for stimulation effects to manifest.

Beyond the specific parameter changes, broader influences on the system's behavior should also be considered. The fact that the other nodes retain the standard Jansen-Rit model values implies that the generated activity may be shaped by additional factors, such as noise, resolution, and stimulation parameters, rather than by changes in the parameter's values of the fundamental differential equations themselves.

A qualitative comparison between the simulated and real EEG signals from the EANSkE project demonstrated similarities, reinforcing the potential of the simulator for studying neurophysiological processes in neurodegenerative diseases. Key similarities include:

- The global signal characteristics closely resemble real EEG activity, reinforcing the biological relevance of the simulation;
- Artifacts in both datasets share similar morphological features, including a main artifact followed by repolarization rise, suggesting that the simulated model captures realistic neural dynamics;
- Evoked responses and their corresponding topographies align well between real and simulated data, further validating the DBS-induced neural activity observed in the model.

This resemblance further strengthens the idea that the simulated DBS response

captures neurophysiological processes, rather than producing an arbitrary computational artifact. The comparison can be made from a purely qualitative point of view since the connectivity patterns of the two subcortical areas stimulated (amygdala and ANT) are different and do not produce the same type of activity. The spatial discrepancy between the artifacts' topoplots is anatomically expected, given that the ANT is a midline structure, whereas the right amygdala is more anteriorly and laterally positioned. This finding supports the physiological realism of the simulated signal, as its electrical activity propagates in a manner consistent with its source location.

The sensitivity analysis identified the most influential parameters in the Jansen-Rit model, revealing how variations in key parameters impact the final model output.

- For the 10k simulation protocol, the most sensitive parameters were B and b ;
- For the 100k simulation protocol, the most sensitive parameters were A and B , with A becoming dominant due to increased sample refinement;
- The change in parameter sensitivity between protocols suggests that increasing the number of simulations and extracted samples leads to a more refined posterior estimation, making the 100k results more reliable.

The eigenvectors shifted, which means that the interactions of the dominant parameters have changed.

The reliability of a protocol depends on the number of simulations it incorporates. Since the second protocol is built from a larger number of simulations, it is inherently more reliable. Key parameters play a crucial role in shaping the outcomes of the study. When reasoning about the A and B values, it is logical to consider them as the two most sensitive parameters in this study.

The interaction between excitatory and inhibitory populations is essential in modifying EPs. Given that the onset of EPs is influenced by this interaction, it makes sense that the relevant model parameters, A and B , would be particularly significant.

These findings provide new insights into the behaviour of the Jansen-Rit model under DBS, demonstrating that:

- The model successfully reproduces key neurophysiological features, making it a strong candidate for further investigations;
- The simulated signal exhibits realistic neural properties, supporting its use in DBS studies and neurophysiological research;
- The sensitivity analysis offers valuable parameter insights, paving the way for future parameter optimization studies.

Given that no prior studies have systematically examined these parameter sensitivities, our findings are novel and provide a foundation for future work. Further research could expand these analyses to additional parameters and explore different stimulation protocols to enhance model precision and applicability.

4.2 Comparison with existing studies

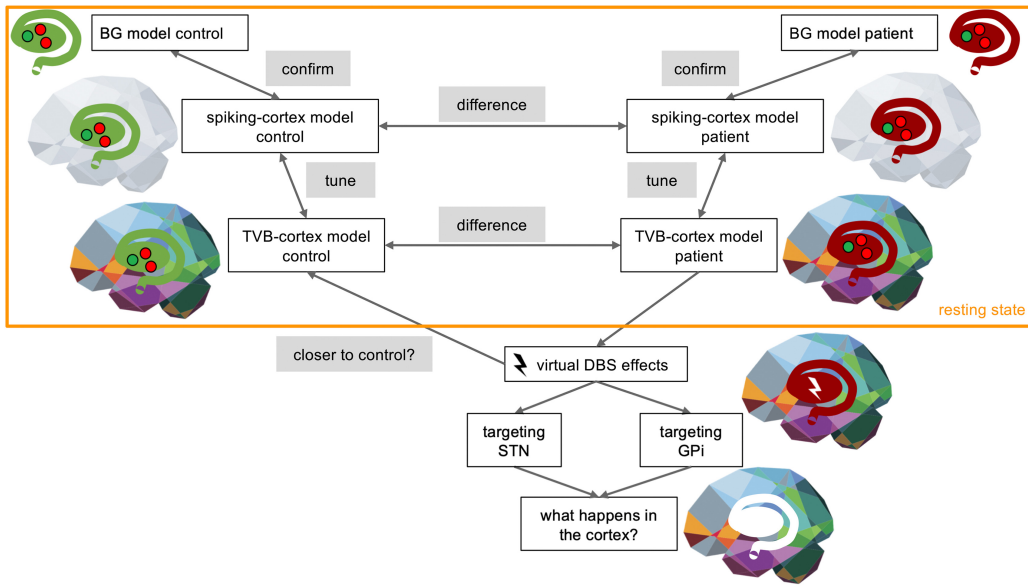


Figure 4.1: Schematic overview of the study design from [Meier *et al.*, 2022]

An important point of reference for this study is the multiscale co-simulation approach introduced by [Meier *et al.*, 2022], which also served as an inspiration for this project.

The study presents a multiscale computational framework that integrates spiking neuron models of the basal ganglia with a whole-brain mean-field model in TVB. This approach enables a comprehensive representation of DBS effects across multiple scales, capturing both local microcircuitry dynamics and global network interactions.

A major finding from their study is that virtual DBS within the model successfully normalizes thalamic activity, shifting it toward a healthy electrophysiological regime. This result aligns with real neurophysiological data, demonstrating the

potential of computational modeling in understanding DBS mechanisms.

The approach provided a key conceptual foundation for our study, particularly in the development of a multiscale computational model using TVB. The central idea inspired the vision of a fully customized treatment framework, where: a DBS model could be co-driven with an epileptic model, allowing for simultaneous investigation of pathological dynamics and therapeutic interventions; MRI-derived signals could serve as the basis for individualized model analyses, tailoring simulations to patient-specific neuroanatomy; and the approach could ultimately facilitate personalized DBS treatment strategies, optimizing stimulation parameters based on neurophysiological feedback from the model.

Some key similarities between [Meier *et al.*, 2022] and the current work include:

- Both studies adopt a multiscale computational approach to investigate DBS mechanisms, use TVB as a central platform for simulating brain dynamics, and aim to bridge the gap between local dynamics and global network effects in DBS;
- The [Meier *et al.*, 2022] study demonstrates that Virtual DBS normalizes thalamic activity, restoring it to a healthy state, and aligning with real electrophysiological data, and also our study aims to investigate how DBS influences pathological dynamics, specifically in the context of epilepsy;
- The long-term vision of both projects includes personalized DBS treatment strategies, where model-based insights guide stimulation parameters.

There are also some key differences, among which:

- In [Meier *et al.*, 2022], the study combines spiking neuron models (microscale) with whole-brain mean-field modeling (macroscale), while our study

uses Jansen-Rit neural mass modeling at the mesoscopic scale within TVB without explicit spiking neuron models;

- In [Meier *et al.*, 2022] DBS effects are modeled at the microscale, while in our study DBS effects are studied at the mesoscale;
- In [Meier *et al.*, 2022], the study requires a co-simulation framework while our study operates entirely within TVB using a single neural mass framework.

So, [Meier *et al.*, 2022] takes a wider multiscale perspective by integrating spiking neuron models with mean-field modeling. This study, on the other hand, focuses on a detailed mesoscale representation using Jansen-Rit neural mass models, making it computationally more efficient while still preserving essential population-level nonlinear interactions. The choice of scale determines the type of insights gained: In [Meier *et al.*, 2022] approach is better suited for studying DBS-induced changes at the microscopic and macroscopic levels. This study is more focused on understanding stimulus-EPs and DBS interactions within cortical columns.

For further comparison, the study by [Wendling *et al.*, 2024] introduces a multiscale neuro-inspired computational modeling framework aimed at interpreting EEG and sEEG signals in epilepsy. The approach integrates three levels of modeling: microscale, mesoscale (NMMs) and macroscale (whole brain). Concerning [Meier *et al.*, 2022] and this study, it emphasizes epilepsy-related biomarkers, such as interictal epileptiform discharges (IEDs), spike-wave patterns, and fast ripples (FRs), to gain mechanistic insights into epileptic activity.

Some key similarities and differences between the studies are:

- All three studies focus on multiscale modeling, linking local neural dynamics to global network behavior: [Wendling *et al.*, 2024] adopt a three-level

approach, while [Meier *et al.*, 2022] integrates spiking models with mean-field models, and this study focuses exclusively on Jansen-Rit NMMs at the mesoscale;

- Both [Wendling *et al.*, 2024] and this study employ Jansen-Rit-based NMMs to simulate cortical column activity, [Meier *et al.*, 2022], in contrast, include spiking neuron models for basal ganglia in their multiscale framework;
- While [Wendling *et al.*, 2024] explicitly model EEG and SEEG signals, which aligns more with this study’s focus on evoked potentials (EPs), [Meier *et al.*, 2022] primarily investigate DBS effects at a network level but do not explicitly model detailed SEEG biomarkers like IEDs.

So, [Meier *et al.*, 2022] offers a DBS-centric multiscale approach, integrating spiking neurons and mean-field models, [Wendling *et al.*, 2024] refine SEEG-based epilepsy modeling, capturing interictal biomarkers at multiple scales and this study focuses on Jansen-Rit modeling of EPs and DBS effects at the mesoscale. Each approach has its unique strengths:

- The study [Meier *et al.*, 2022] provide a spiking-macroscale DBS framework;
- The study [Wendling *et al.*, 2024] offer a multi-layered neocortical model for interpreting epilepsy-related EEG signals;
- This study remains within the mesoscale Jansen-Rit framework, making it computationally efficient while relevant for DBS-EP interactions.

We were thus able to observe a comparison of different multiscale models for different purposes and contexts.

4.3 Limitations and Future Work

As with any computational model, this project inherently involves simplifications of complex neural phenomena. These approximations, while necessary for feasibility, introduce certain limitations that should be considered when computing the simulations and interpreting the results.

One of the fundamental limitations of the project arises from the use of the Jansen-Rit NMM itself, which, as generally true for every other NMM, does not simulate the activity of individual neurons but instead models the average dynamics of neural populations. By neglecting microscopic neuronal variability, the model assumes homogeneous neural population dynamics, represented by differential equations. While this provides a computationally efficient approach, it inherently simplifies the richness of real neural activity.

Both the TVB framework and Jansen-Rit employ simplified coupling equations to approximate neural interactions across different brain regions. Jansen-Rit, for example, assumes a sigmoidal response function $\text{sigm}(v)$ (Eq. 1.3) to approximate real nonlinear neural interactions with a transfer function, while brain regions in TVB are assumed to be single nodes (and so inherently homogeneous) neglecting that each brain region has subdivisions with heterogeneous connectivity patterns.

A key limitation in this study was the inability to generate a patient-specific connectivity matrix due to logistical constraints. Instead, we relied on TVB's default connectivity matrix which limits patient-specific accuracy. This is because among the datasets available with the TVB software, there was a connectivity matrix with the thalamus, but its projections were disconnected and generated no response regardless of the stimulation that prompted it. Therefore, the only dataset with the right amygdala available as a subcortical zone had to be used.

While our DBS simulations targeted the right amygdala, the effects of stimulat-

ing this region are not directly comparable to ANT stimulation due to differences in connectivity patterns: the amygdala is involved in limbic processing and emotional regulation, with its primary projections on the hippocampus and prefrontal cortex [Salzman and Fusi, 2010]. ANT, differently, plays a crucial role in thalamocortical loops [Child and Benarroch, 2013]. For these reasons, stimulation of the amygdala does not directly reproduce the same network effects as ANT stimulation. Due to this, we decided not to perform a parametric reconstruction of the evoked responses via SBI of the model parameters as it would not have had a solid enough theoretical basis.

Lastly, TVB uses a forward model to project neural activity onto scalp electrodes. This means that there are volume conduction models that do not perfectly capture the real biophysical properties of the head.

Future work could involve refining the computational model with the addition of more biologically realistic parameters or supplementary neural populations. Eventually, integrating patient-specific MRI data could allow for individualized tuning of EEG activity, potentially improving the accuracy of simulated responses. Validation of the refined model against empirical electrophysiological data could further enhance its reliability.

Once a customised connectome is obtained, this study is considered to have a ready-to-use pipeline for data reconstruction via clinical dataset and the possibility of customisation of treatment.

Conclusion

This study validates the integration of the Jansen-Rit NMM within a complex multiscale neural network framework, i.e., the TVB. A sanity check was performed to ensure that the model accurately reproduced the fundamental neural activities described in its original formulation.

Beyond validation, this research confirms the neurophysiological relevance of a multiscale computational approach in studying the effects of DBS on whole-brain dynamics. The framework successfully generated plausible evoked responses to virtual DBS, demonstrating its potential as a valuable tool for investigating epilepsy treatment mechanisms.

The biological and neurophysiological plausibility of the model is further reinforced through a direct qualitative comparison with real data from EANSkE. This comparison highlights a strong resemblance between the simulated results and empirical data, particularly in terms of GMFP, stimulation artifacts, and topographic distributions.

A sensitivity analysis provides deeper insights into the model's behaviour by identifying key parameters that strongly influence the output. This analysis reveals a marked sensitivity of the system to specific parameter variations, opening new avenues for research into the relationship between intrinsic model properties and

observed neural responses.

Future work aims to enhance the model's applicability through the integration of patient-specific neural connectivity data derived from MRI. This advancement would enable the framework to serve as a customizable platform, requiring minimal adaptation to tailor simulations to individual subjects.

A customized connectome based on MRI scans plays a crucial role in enhancing neuromodulation strategies for refractory epilepsy. Once the integration of this connectome is complete, the project demonstrates its readiness and functionality as a reliable pipeline. This ensures that the system can be effectively applied to improve treatment outcomes for patients with refractory epilepsy.

Acknowledgements

Looking back at the path I chose and the decisions that brought me here, I have no regrets about dedicating myself to this thesis. My passion for neuroscience carried me through even when I doubted myself, and this journey has been a profound learning experience culturally, intellectually, and professionally. However, I could not have done this alone, and I would like to express my gratitude to those who supported me along the way.

First and foremost, I extend my deepest thanks to my supervisor, Maria Carla. You gave me an opportunity that many others might not have, and for that, I am truly grateful. You have been my Obi-Wan Kenobi, guiding me through challenges and pushing me beyond boundaries I didn't even realize existed. Thank you for believing in me, for testing me, and for helping me grow. I sincerely hope our paths cross again in the future.

I am also deeply grateful to Professor Martinoia, whose support made it possible for me to collaborate with the University of Twente. Without him, none of this would have been possible.

Thank you to Nadya, an incredible co-supervisor who was always ready to help, problem-solve, and provide unwavering support. Your guidance and encouragement made a difference.

And thank you,

To my mum, who may not have understood everything I said but still managed to cry from the moment I uttered, "Good morning, everyone...". Thank you for teaching me, as a woman, what it means to be a man.

To my dad for teasing me and challenging me morally at every failure, rather than simply stopping me from playing video games (though, of course, you did that too). Thank you for our endless conversations about engineering, mathematics, and physics over dinner.

To my sister, who welcomed me into her home without hesitation, as if it were my own. Our differences bring us closer, not further apart. May the force be with you sister. I am officially a Jedi Master.

To all my friends, the few who had the courage (or perhaps the lack of common sense) to stand by me, no matter my choices.

And to my Simona, you are everything beautiful in life. I would follow you to the ends of the earth. You have proof of that.

Finally, never play for the audience, play for yourselves.

Bibliography

- [Benbadis, 2009] S. Benbadis. *The differential diagnosis of epilepsy: A critical review*. Epilepsy & Behavior, 2009.
- [Bromfield *et al.*, 2006] E.B. Bromfield, J.E. Cavazos, and J.I. Sirven. *An Introduction to Epilepsy, Chapter 1*. West Hartford (CT): American Epilepsy Society, 2006.
- [Case and Soltesz, 2011] M. Case and I. Soltesz. *Computational modeling of epilepsy*. Epilepsia, 2011.
- [Challenor *et al.*, 1994] Y. Challenor, E. Gonzalez, and A. Cassvan. *Evoked potentials*. The Physiological Basis of Rehabilitation Medicine, 1994.
- [Child and Benaroch, 2013] N.D. Child and E.E. Benaroch. *Anterior nucleus of the thalamus: functional organization and clinical implications*. Neurology, 2013.
- [Cleveland Clinic, 2022] Cleveland Clinic. Epilepsy: What it is, causes, symptoms & treatment, 2022.
- [Constantine *et al.*, 2014] P. G. Constantine, E. Dow, and Q. Wang. *Active Subspace Methods in Theory and Practice: Applications to Kriging Surfaces*. Society for Industrial & Applied Mathematics (SIAM), 2014.

- [Dale *et al.*, 1999] A.M. Dale, B. Fischl, and M.I. Sereno. *Cortical Surface-Based Analysis: I. Segmentation and Surface Reconstruction*. NeuroImage, 1999.
- [Dale *et al.*, 2022] J. Dale, S.L. Schmidt, K. Mitchell, and W.M. Turner. *Evoked potentials generated by deep brain stimulation for Parkinson's disease*. Brain stimulation, 2022.
- [Fifer *et al.*, 2006] W. P. Fifer, P.G. Grieve, J. Grose-Fifer, J.R. Isler, and D. Byrd. *High-Density Electroencephalogram Monitoring in the Neonate*. Clinics in Perinatology, 2006.
- [Fisher *et al.*, 2010] R. Fisher, V. Salanova, and T. Witt. *Electrical stimulation of the anterior nucleus of thalamus for treatment of refractory epilepsy*. Epilepsia, 2010.
- [Fisher, 2017] R.S. Fisher. *The New Classification of Seizures by the International League Against Epilepsy 2017*. Curr Neurol Neurosci Rep, 2017.
- [Foutz and Wong, 2022] T.J. Foutz and M. Wong. *Brain stimulation treatments in epilepsy: Basic mechanisms and clinical advances*. Biomedical journal, 2022.
- [Fox *et al.*, 2014] M.D. Fox, R.L. Buckner, H. Liu, M.M. Chakravarty, A.M. Lozano, and A. Pascual-Leone. *Resting-state networks link invasive and non-invasive brain stimulation across diverse psychiatric and neurological diseases*. Proc. Natl. Acad. Sci. U.S.A., 2014.
- [Goldstein and Slomski, 2008] J. Goldstein and J. Slomski. *Epileptic spasms: a variety of etiologies and associated syndromes*. J Child Neurol, 2008.
- [González *et al.*, 2019] H.F.J. González, A. Yengo-Kahn, and D.J. Englot. *Vagus Nerve Stimulation for the Treatment of Epilepsy*. Neurosurgery clinics of North America, 2019.

- [Gonçalves and Lueckmann, 2020] P.J. Gonçalves and J. Lueckmann. *Training deep neural density estimators to identify mechanistic models of neural dynamics*. eLife Sciences Publications, 2020.
- [Haueis, 2022] P. Haueis. Descriptive multiscale modeling in data-driven neuroscience. *Synthese*, 2022.
- [Jansen and Rit, 1995] B.H. Jansen and V.G. Rit. *Electroencephalogram and visual evoked potential generation in a mathematical model of coupled cortical columns*. Biol. Cybern., 1995.
- [Jirsa and Stefanescu, 2011] V. Jirsa and R. Stefanescu. *Neural population modes capture biologically realistic large scale network dynamics*. Bulletin of mathematical biology, 2011.
- [Jobst *et al.*, 2010] B.C. Jobst, T.M. Darcey, and V.M. Thadani. *Brain stimulation for the treatment of epilepsy*. Epilepsia, 2010.
- [Kirchner *et al.*, 2020] A. Kirchner, F. Dachet, and J.A. Loeb. *Identifying targets for preventing epilepsy using systems biology of the human brain*. Neuropharmacology, 2020.
- [Kirschstein and Köhling, 2009] T. Kirschstein and R. Köhling. *What is the Source of the EEG?* Clinical EEG and Neuroscience, 2009.
- [Krey *et al.*, 2022] I. Krey, K. Platzer, A. Esterhuizen, and S.F. Berkovic. *Current practice in diagnostic genetic testing of the epilepsies*. Epileptic Disorders, 2022.
- [LaBerge and Kasevich, 2017] D. LaBerge and R.S. Kasevich. *Neuroelectric Tuning of Cortical Oscillations by Apical Dendrites in Loop Circuits*. Front. Syst. Neurosci., 2017.

[Laxpati *et al.*, 2014] N.G. Laxpati, W.S. Kasoff, and R.E. Gross. *Deep brain stimulation for the treatment of epilepsy: circuits, targets, and trials*. Neurotherapeutics, 2014.

[Litvak *et al.*, 2021] V. Litvak, E. Florin, G. Tamás, and S. Groppa. *EEG and MEG primers for tracking DBS network effects*. NeuroImage, 2021.

[Loosveld, 2024] L.H.G. Loosveld. Source reconstruction of ant-dbs induced evoked potentials and epileptiform discharges in patients with refractory epilepsy, 2024.

[Mahrouss *et al.*, 2025] A.A. Mahrouss, L. Liang, and J.M. Balaguer. *Pharmacological blocking of spinal GABA_A receptors in monkeys reduces sensory transmission to the spinal cord, thalamus, and cortex*. Cell Rep., 2025.

[Mayo Clinic, 2023] Mayo Clinic. Epilepsy - symptoms and causes, 2023.

[Mayo Clinic, 2024] Mayo Clinic. Vagus nerve stimulation, 2024.

[McIntyre and Anderson, 2016] C.C. McIntyre and R.W. Anderson. *Deep brain stimulation mechanisms: the control of network activity via neurochemistry modulation*. Journal of Neurochemistry, 2016.

[Meier *et al.*, 2022] J.M. Meier, D. Perdikis, A. Blickensdörfer, L. Stefanovski, Q. Liu, O. Maith, H.Ü. Dinkelbach, J. Baladron, F.H. Hamker, and P. Ritter. *Virtual deep brain stimulation: Multiscale co-simulation of a spiking basal ganglia model and a whole-brain mean-field model with The Virtual Brain*. Experimental Neurology, 2022.

[National Institute of Neurological Disorders and Stroke, 2025] National Institute of Neurological Disorders and Stroke. Epilepsy and seizures, 2025.

[Odekerken *et al.*, 2015] V.J.J. Odekerken, J.A. Boel, and G.J. Geurtzen. *Neuropsychological outcome after deep brain stimulation for Parkinson disease*. *Neurology*, 2015.

[Oostenveld *et al.*, 2011] R. Oostenveld, P. Fries, E. Maris, and J. Schoffelen. *FieldTrip: Open Source Software for Advanced Analysis of MEG, EEG, and Invasive Electrophysiological Data*. Computational Intelligence and Neuroscience, 2011.

[Pelinen *et al.*, 2024] J. Pelinen, C.E. Foster, J.M. Wilmhurst, S.M. Zuberi, and J. French. *Improving epilepsy diagnosis across the lifespan: approaches and innovations*. *The Lancet Neurology*, 2024.

[Proix *et al.*, 2016] T. Proix, A. Spiegler, M. Schirner, S. Rothmeier, P. Ritter, and V.K. Jirsa. *How do parcellation size and short-range connectivity affect dynamics in large-scale brain network models?* *NeuroImage*, 2016.

[Rho *et al.*, 2010] J. Rho, R. Sankar, and C.E. Stafstrom. *Epilepsy: mechanisms, models, and translational perspectives*. CRC Press, 2010.

[Richardson, 2012] M.P. Richardson. *Large scale brain models of epilepsy: dynamics meets connectomics*. BMJ Publishing Group Ltd, 2012.

[Salanova *et al.*, 2015] V. Salanova, T. Witt, and R. Worth. *Long-term efficacy and safety of thalamic stimulation for drug-resistant partial epilepsy*. *Neurology*, 2015.

[Salanova *et al.*, 2021] V. Salanova, M.R. Sperling, and R.E. Gross. *The SANTE study at 10 years of follow-up: Effectiveness, safety, and sudden unexpected death in epilepsy*. *Epilepsia*, 2021.

[Salzman and Fusi, 2010] C.D. Salzman and S. Fusi. *Emotion, cognition, and mental state representation in amygdala and prefrontal cortex*. Annual review of neuroscience, 2010.

[Sanz-Leon *et al.*, 2015] P. Sanz-Leon, S.A. Knock, A. Spiegler, and V.K. Jirsa. *Mathematical framework for large-scale brain network modeling in The Virtual Brain*. NeuroImage, 2015.

[Scheffer *et al.*, 2017] I.E. Scheffer, S. Berkovic, and G. Capovilla. *ILAE classification of the epilepsies: Position paper of the ILAE Commission for Classification and Terminology*. Epilepsia, 2017.

[Schneeweiss *et al.*, 2006] S. Schneeweiss, S. Berkovic, and G. Capovilla. *Sensitivity analysis and external adjustment for unmeasured confounders in epidemiologic database studies of therapeutics*. Pharmacoepidem. Drug Safe., 2006.

[Schwalger *et al.*, 2017] T. Schwalger, M. Deger, and W. Gerstner. *Towards a theory of cortical columns: From spiking neurons to interacting neural populations of finite size*. PLoS computational biology, 2017.

[Skodda, 2012] S. Skodda. *Effect of Deep Brain Stimulation on Speech Performance in Parkinson’s Disease*. Parkinson’s Disease, 2012.

[Stafstrom and Carmant, 2015] C.E. Stafstrom and L. Carmant. *Seizures and epilepsy: an overview for neuroscientists*. Cold Spring Harb Perspect Med., 2015.

[Strzelczyk *et al.*, 2023] A. Strzelczyk, A. Aledo-Serrano, A. Coppola, A. Didelot, E. Bates, R. Sainz-Fuertes, and C. Lawthom. *The impact of epilepsy on quality of life: Findings from a European survey*. Epilepsy & Behavior, 2023.

[Thabane *et al.*, 2013] L. Thabane, L. Mbuagbaw, and S. Zhang. *A tutorial on sensitivity analyses in clinical trials: the what, why, when and how*. BMC Med Res Methodol, 2013.

[Viel *et al.*, 1995] J.F. Viel, D. Pobel, and A. Carré. *Incidence of leukaemia in young people around the La hague nuclear waste reprocessing plant: A sensitivity analysis*. Statist. Med., 1995.

[Wang *et al.*, 2020] Y. Wang, V. Kremen, B.H. Brinkmann, E.H. Middlebrooks, and B.N. Lundstrom. *Probing circuit of Papez with stimulation of anterior nucleus of the thalamus and hippocampal evoked potentials*. Epilepsy Research, 2020.

[Wendling *et al.*, 2024] F. Wendling, E. Koksal-Ersoz, M. Al-Harrach, M. Yochum, I. Merlet, G. Ruffini, F. Bartolomei, and P. Benquet. *Multiscale neuro-inspired models for interpretation of EEG signals in patients with epilepsy*. Clinical Neurophysiology, 2024.

[Wiebe and Jette, 2012] S. Wiebe and N. Jette. *Pharmacoresistance and the role of surgery in difficult to treat epilepsy*. Nat Rev Neurol, 2012.

[Yu *et al.*, 2018] T. Yu, X. Wang, Y. Li, G. Zhang, G. Worrell, and P. Chauvel. *High-frequency stimulation of anterior nucleus of thalamus desynchronizes epileptic network in humans*. Brain, 2018.

Appendix

Connectivity reconstruction with SCRIPTS

In this project, we attempted to reconstruct a personalized connectivity matrix using MRI data from patient DBS007. This process was carried out using the Surface and Connectivity Reconstruction: Imaging Pipeline for TVB Simulations (SCRIPTS), a specialized software framework designed to prepare structural and functional imaging data for integration into TVB available at the link <https://github.com/ins-amu/scripts> and whom workflow can be seen in Figure 6.1.

Despite our efforts, we were unable to achieve the desired connectivity reconstruction due to technical difficulties in running the pipeline with MRtrix <https://www.mrtrix.org/>.

Research explores the emergence of normal and altered functional brain states on a large scale: resting state networks (RSNs) have been related to large-scale structural connectivity using whole-brain models, epileptic seizures have been associated with large-scale network dysfunction and non-invasive brain stimulation is seen as a promising tool to affect large-scale networks during treatments of neurological and psychiatric disorders [Richardson, 2012] [Fox *et al.*, 2014].

BNMs integrate structural data gathered from MRI or dMRI to describe the connectivity of brain areas at large scales using reconstruction softwares [Proix *et*

al., 2016].

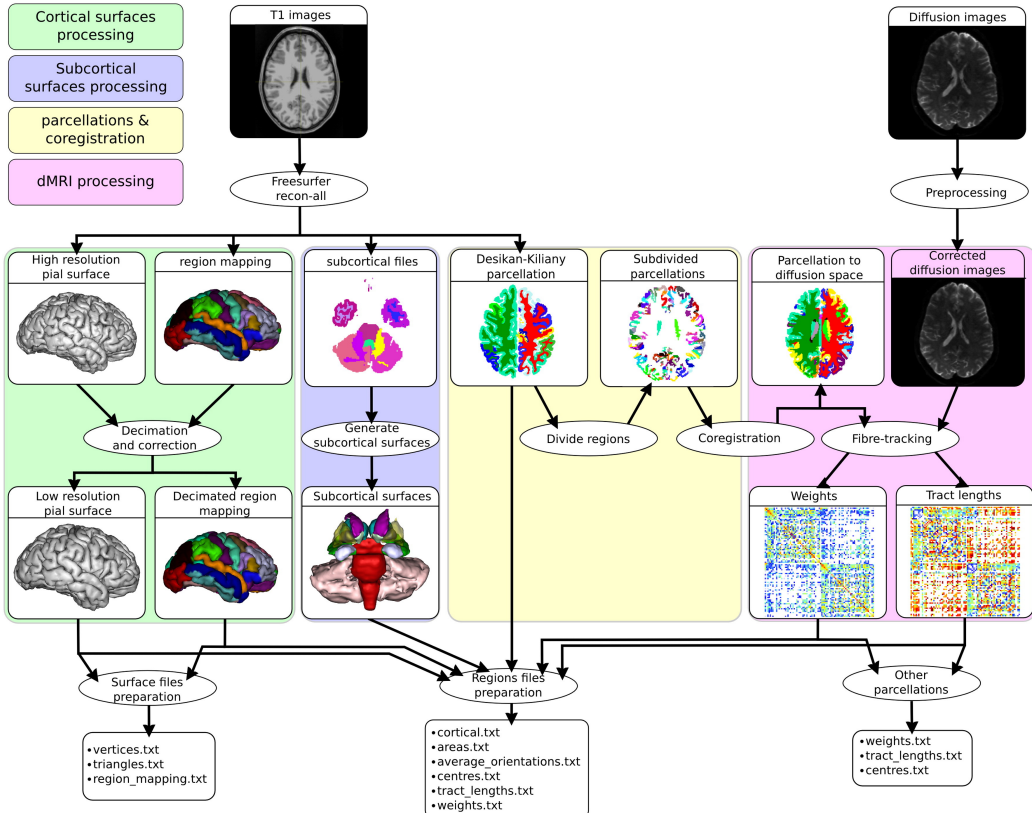


Figure 6.1: Overview of the workflow for cortical and subcortical surfaces processing, parcellations and co-registration, and dMRI processing from [Proix *et al.*, 2016]

The SCRIPTS pipeline follows a two-step process:

- A surface reconstruction (Figure 6.2a) through T1-weighted structural scan of a subject using FreeSurfer [Dale *et al.*, 1999];
- Heterogeneous connectivity reconstruction with dMRI data.

Once the surface and connectivity reconstruction steps are completed, the

SCRIPTS pipeline generates files formatted for direct upload into the TVB framework.

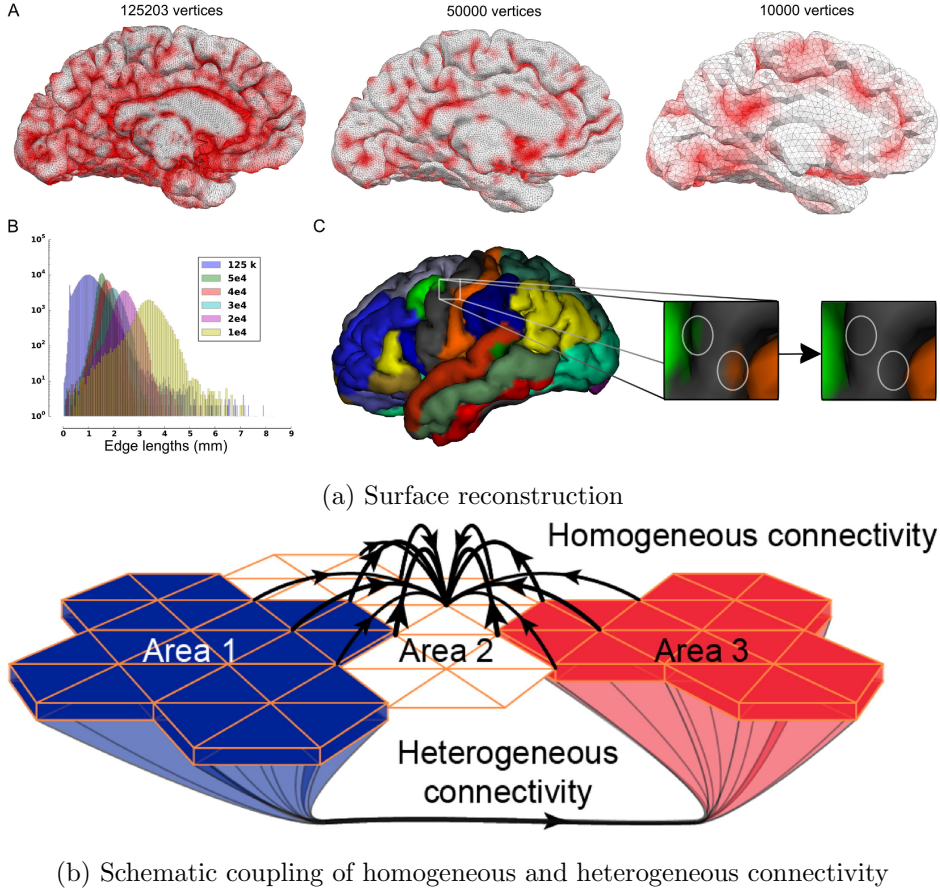


Figure 6.2: Surface reconstruction and schematic coupling of connectivity from [Proix *et al.*, 2016]

By successfully integrating these datasets, TVB simulations can incorporate personalized brain connectivity, enhancing the realism and interpretability of network-level analyses. Although technical difficulties prevented full implementation, this exploration of SCRIPTS-based connectivity reconstruction highlights its potential for personalized TVB modeling. By refining these methods, we can move closer

to a fully patient-specific brain simulation framework, ultimately improving DBS modeling and clinical applicability.

Generic Bi-dimensional Oscillator

As an initial step in understanding the TVB framework, our first simulations were conducted using a generic bi-dimensional oscillator model as a baseline for our multiscale framework. This model provided a simplified representation of neural dynamics, allowing us to explore fundamental oscillatory behaviors before transitioning to more complex models. We can grasp a definition of this bi-dimensional oscillator directly from the module on the TVB website https://docs.thevirtualbrain.org/_modules/tvb/simulator/models/oscillator.html and from the related paper [Sanz-Leon *et al.*, 2015]:

”The generic bi-dimensional oscillator model is a generic dynamic system with two state variables. The dynamic equations of this model are composed of two ordinary differential equations comprising two nullclines. The first nullcline is a cubic function as it is found in most neuron and population models; the second nullcline is arbitrarily configurable as a polynomial function up to second order. The manipulation of the latter nullcline’s parameters allows to generate a wide range of different behaviours”.

The bi-dimensional oscillator is a generic dynamical system with two state variables, governed by the following differential equations:

$$\dot{V} = d\tau(-fV^3 + eV^2 + gV + \alpha W + \gamma I) \quad (6.1)$$

$$\dot{W} = \frac{d}{\tau}(cV^2 + bV - \beta W + a) \quad (6.2)$$

$$(6.3)$$

While this model can be useful to study different type of behaviours, among

which we can cite the global oscillatory behaviour, resting-state activity or the large-scale dynamics of the brain, for our purposes it presented some limitations regarding the study of EPs which diverted us towards finding an alternative model to use, which turned out to be Jansen-Rit:

- There is no direct modeling of synaptic interactions and neural mass activity at the mesoscopic scale;
- Unlike Jansen-Rit, it does not explicitly represent excitatory and inhibitory populations in cortical circuits;
- Generally speaking, it is not specifically designed to model stimulus-evoked responses.

We have shown, on the other side, that the Jansen-Rit model is a neural mass model explicitly designed to simulate cortical column activity, and being so, it is more appropriate for studying evoked potentials in response to stimulation:

- Having three interacting neural populations, it provides a biologically plausible mechanism for EP generation;
- Unlike simple oscillators, it describes and exhibits nonlinear interactions between the different neural populations, crucial for studying stimulus-driven dynamics;
- The model directly outputs electrical potentials that are relatable to EEG recordings, instead of abstract phase oscillators.

While the generic bi-dimensional oscillator provided a useful introduction to neural modeling, its inability to capture synaptic interactions, stimulus-evoked responses, and realistic cortical activity made it unsuitable for our specific objectives. This transition was essential for enhancing the realism and applicability of

our simulations, ultimately leading to a more robust framework for understanding DBS-induced neural responses.